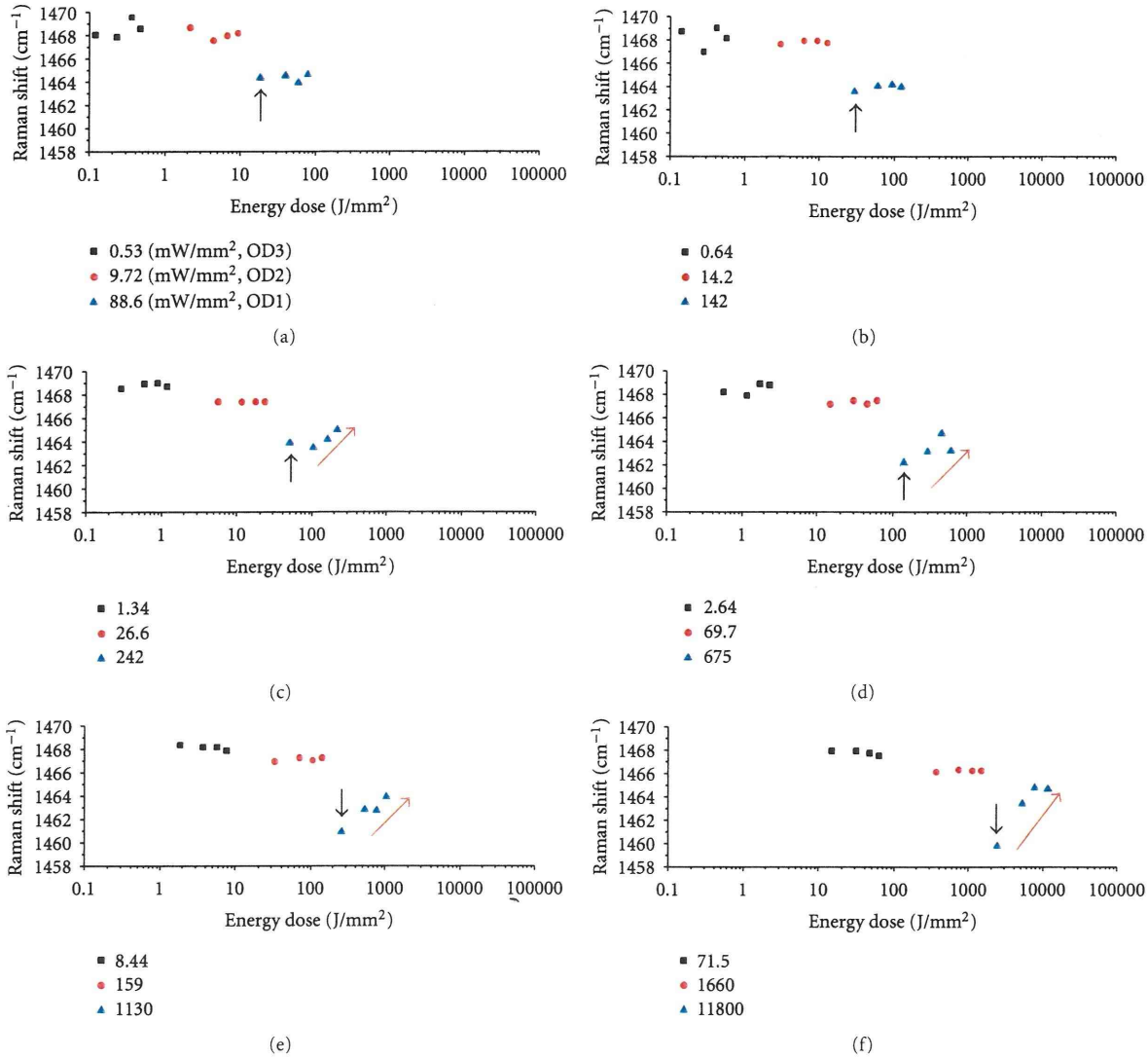

FIGURE 6: $A_g(2)$ peak positions of the Raman spectra of C_{60}NWs under various exposure conditions at the defocus values of (a) 100 μm, (b) 80 μm, (c) 60 μm, (d) 40 μm, (e) 20 μm, and (f) 0 μm (just focus), corresponding to (a) ~ (f) of **Figure 3**.

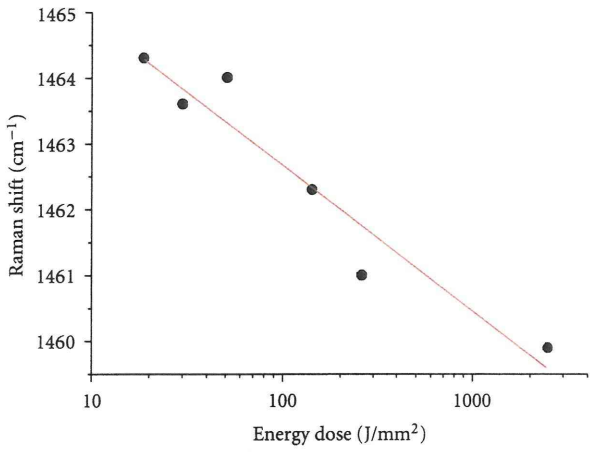

FIGURE 7: Relationship between the Raman shift of $A_g(2)$ peak and the energy dose of C_{60}NWs irradiated by the excitation laser beams.

C_{60} molecules are linearly polymerized by forming the four-membered rings along the growth axis of C_{60}NWs, as was shown in **Figure 6** of [2].

In the gas chromatography-mass spectrometry (GC-MS) measurement of solvents contained in the C_{60}NWs that were prepared by use of toluene and IPA, the major residual solvent was toluene, and the content of IPA was very small compared with toluene [14]. Since the residual toluene of C_{60}NWs was measured to be about 0.2% after drying in an Ar atmosphere at 100°C for 30 min. [14], it is considered that the residual toluene of the vacuum-dried samples of C_{60}NWs in the present experiment is negligible and does not influence the Raman profiles.

4. Conclusions

The photopolymerization of C_{60}NWs was investigated by using the Raman laser beam of 532 nm wavelength at various

exposure conditions for the power density and the exposure time in air.

The $A_g(2)$ peak of C_{60}NWs shifted to the lower wavenumbers from that of the as-grown dried C_{60}NWs. However, the $A_g(2)$ peaks were found to move to the higher wavenumbers from the polymerized positions by the irradiation of laser beams for high energy doses at high-power densities, indicating the thermal dissociation of polymerized C_{60} molecules owing to the temperature rise.

An energy dose larger than about 1520 J/mm^2 was found to be necessary for the laser beam of 532 nm wavelength to obtain the photopolymerized C_{60}NWs.

Acknowledgment

Part of this research was supported by Health and Labour Sciences Research Grants (H21-Chemistry-Ippan-008) from the Ministry of Health, Labour, and Welfare of Japan.

References

[1] K. Miyazawa, "Synthesis and properties of fullerene nanowhiskers and fullerene nanotubes," *Journal of Nanoscience and Nanotechnology*, vol. 9, no. 1, pp. 41–50, 2009.

[2] K. Miyazawa, Y. Kuwasaki, A. Obayashi, and M. Kuwabara, "C_{60} nanowhiskers formed by the liquid-liquid interfacial precipitation method," *Journal of Materials Research*, vol. 17, no. 1, pp. 83–88, 2002.

[3] K. Ogawa, T. Kato, A. Ikegami et al., "Electrical properties of field-effect transistors based on C_{60} nanowhiskers," *Applied Physics Letters*, vol. 88, no. 11, Article ID 112109, 3 pages, 2006.

[4] P. R. Somani, S. P. Somani, and M. Umeno, "Toward organic thick film solar cells: three dimensional bulk heterojunction organic thick film solar cell using fullerene single crystal nanorods," *Applied Physics Letters*, vol. 91, no. 17, Article ID 173503, 3 pages, 2007.

[5] X. Zhang, Y. Qu, G. Piao, J. Zhao, and K. Jiao, "Reduced working electrode based on fullerene C_{60} nanotubes@DNA: characterization and application," *Materials Science and Engineering B*, vol. 175, no. 2, pp. 159–163, 2010.

[6] M. Nakaya, T. Nakayama, and M. Aono, "Fabrication and electron-beam-induced polymerization of C_{60} nanoribbon," *Thin Solid Films*, vol. 464-465, pp. 327–330, 2004.

[7] M. Tachibana, K. Kobayashi, T. Uchida, K. Kojima, M. Tanimura, and K. Miyazawa, "Photo-assisted growth and polymerization of C_{60} "nano"whiskers," *Chemical Physics Letters*, vol. 374, no. 3-4, pp. 279–285, 2003.

[8] K. Miyazawa, J. Minato, M. Fujino, and T. Suga, "Structural investigation of heat-treated fullerene nanotubes and nanowhiskers," *Diamond and Related Materials*, vol. 15, no. 4–8, pp. 1143–1146, 2006.

[9] K. Asaka, R. Kato, K. Miyazawa, and T. Kizuka, "Buckling of C_{60} whiskers," *Applied Physics Letters*, vol. 89, no. 7, Article ID 071912, 3 pages, 2006.

[10] D. Koide, S. Kato, E. Ikeda, N. Iwata, and H. Yamamoto, "Free electron laser-polymerization of C_{60} grown by liquid-liquid-interfacial precipitation method," *IEICE Transactions on Electronics*, vol. 94, no. 2, pp. 151–156, 2011.

[11] A. M. Rao, P. Zhou, K. A. Wang et al., "Photoinduced polymerization of solid C_{60} films," *Science*, vol. 259, no. 5097, pp. 955–957, 1993.

[12] E. Alvarez-Zauco, H. Sobral, E. V. Basiuk, J. M. Saniger-Blesa, and M. Villagrán-Muniz, "Polymerization of C_{60} fullerene thin films by UV pulsed laser irradiation," *Applied Surface Science*, vol. 248, no. 1–4, pp. 243–247, 2005.

[13] Y. Wang, J. M. Holden, X. X. Bi, and P. C. Eklund, "Thermal decomposition of polymeric C_{60}," *Chemical Physics Letters*, vol. 217, no. 4, pp. 413–417, 1994.

[14] M. Watanabe, K. Hotta, K. Miyazawa, and M. Tachibana, "GC-MS analysis of the solvents contained in C_{60} nanowhiskers," *Journal of Physics: Conference Series*, vol. 159, no. 1, Article ID 012010, 2009.

The Journal of Toxicological Sciences (J. Toxicol. Sci.)
Vol.37, No.2, 317-327, 2012

Original Article

Lack of promoting effect of titanium dioxide particles on chemically-induced skin carcinogenesis in rats and mice

Yoko Sagawa[1,2], Mitsuru Futakuchi[2], Jiegou Xu[2,3], Katsumi Fukamachi[2], Yuto Sakai[2,4], Yoshiaki Ikarashi[5], Tetsuji Nishimura[5], Masumi Suzui[2], Hiroyuki Tsuda[3] and Akimichi Morita[1]

[1]Department of Geriatric and Environmental Dermatology and [2]Department of Molecular Toxicology, Nagoya City University Graduate School of Medical Sciences, 1-Kawasumi, Mizuho-cho, Mizuho-ku, Nagoya 467-8601, Japan
[3]Nanotoxicology Project Laboratory, Nagoya City University and [4]Department of Drug Metabolism and Disposition, Nagoya City University Graduate School of Pharmaceutical Sciences, 3-1 Tanabedohri, Mizuho-ku, Nagoya 467-8603, Japan
[5]Division of Environmental Chemistry, National Institute of Health Sciences, 1-18-1 Kamiyoga, Setagaya-ku, Tokyo 158-8501, Japan

(Received December 5, 2011; Accepted December 27, 2011)

ABSTRACT — Nano-sized titanium dioxide particles (TiO_2) are widely used in cosmetics, sunscreens and food additives. We previously reported that topical application of non-coated rutile type TiO_2 did not exhibit a promoting effect on ultraviolet B-initiated skin carcinogenesis in rats, and that this was likely due to lack of penetration of TiO_2 into the epidermis. In the present study, we examined the promoting effect of silicone coated TiO_2 ($sTiO_2$) suspended in silicone oil and non-coated TiO_2 ($ncTiO_2$) suspended in Pentalan 408 on a two-stage skin chemical carcinogenesis model: $sTiO_2$ suspended in silicon oil forms smaller particles than $ncTiO_2$ suspended in Pentalan because of the smaller sizes of aggregates formed. The model used skin carcinogenesis-sensitive human c-Ha-ras proto-oncogene transgenic mice (rasH2) and rats (Hras128) and their wild-type counterparts and CD-1 mice to test the effects of topical application of TiO_2. Animals were initially treated with a single dose of 7,12-dimethylbenz[a]anthracene (DMBA) and then with 0, 10, or 20 mg $sTiO_2$ (mice) or 0, 50, or 100 mg $ncTiO_2$ (rats). The incidence and multiplicity of skin tumors (squamous cell papilloma and carcinoma) did not increase over DMBA alone controls in skin carcinogenesis-sensitive mice or rats or wild-type animals. Analysis of rat skin indicated that $sTiO_2$ and $ncTiO_2$ did not penetrate though either healthy or damaged skin. Furthermore $sTiO_2$ did not penetrate an *in vitro* human epidermis model. Our results indicate that treatment with $sTiO_2$ or $ncTiO_2$ did not promote skin carcinogenesis in mice or rats, probably due to lack of penetration through the epidermis.

Key words: Nano-size TiO_2, Skin carcinogenesis, Hras, Rat, Mouse

INTRODUCTION

Nano-sized titanium dioxide (TiO_2) particles are used in sunscreen formulations to protect against skin lesions caused by exposure to UV light (Gelis *et al.*, 2003; Rouabhia *et al.*, 2002; Suzuki, 1987). Nano and larger scale titanium dioxide particles are known to be carcinogenic to the rat lung (Baan *et al.*, 2006; Baan, 2007). Recently, we demonstrated a promoting effect on rat lung carcinogenesis by nano-size TiO_2 particles administered by a novel intrapulmonary spraying method (Xu *et al.*, 2010). The mechanism of promotion of lung carcinogenesis involved the induction of MIP1α protein expression by $ncTiO_2$-laden alveolar macrophages (Xu *et al.*, 2010).

We also examined the carcinogenic effect of TiO_2 (mean manufacturer's particulate diameter of 20 nm) on the skin in a UVB-initiated two-stage rat carcinogenesis model and found that topical application of TiO_2 did not promote skin carcinogenesis in this model. This result is probably due to the inability of TiO_2 to penetrate through

Correspondence: Akimichi Morita (E-mail: amorita@med.nagoya-cu.ac.jp)

the epidermis and reach the underlying tissue (Xu *et al.*, 2011). This speculation is consistent with a report by Newman *et al.* (2009) demonstrating an absence of penetration of TiO_2 through the epidermis and hair follicles (Newman *et al.*, 2009). On the other hand, Wu *et al.* (2009) reported that TiO_2 (4 nm and 60 nm length) could penetrate through the stratum corneum (SC) and become located in the deep layer of the epidermis after being topically applied to pig ear for 30 days (Wu *et al.*, 2009). These inconsistent observations may be due to differences in particle size and the animals used.

The skin is histologically composed of the SC, epidermis, dermis and the subcutaneous tissue. The SC is the rate-limiting barrier against exposure to various exogenous chemical and physical agents (Schaefer *et al.*, 2003). For solid materials, including nano-sized particles, to cause inflammatory lesions, they need to penetrate the SC to interact with macrophages and other inflammatory leucocytes. Long-term activation of inflammatory leukocytes has the potential to cause skin carcinogenesis. Thus, the potential skin-carcinogenicity of TiO_2 is dependent on its size and ability to penetrate through the SC.

The surface of the TiO_2 used in cosmetics is usually coated with aluminum oxide or silicone oils to prevent aggregate formation and to enhance dispersal (Nohynek *et al.*, 2008). The particle size of TiO_2 suspended in silicone oils is known to be smaller than that of non-coated TiO_2 suspensions (Senzui *et al.*, 2010; also compare Fig. 1E with Fig. 1F). In our previous study, we showed that rutile type non-coated TiO_2 ($ncTiO_2$) did not penetrate the epidermal tissue and thus did not cause promotion of chemically-induced skin carcinogenesis. In the present study, we used rutile type TiO_2 coated with silicone ($sTiO_2$) suspended in silicon oil to minimize aggregation and improve the penetrating ability of the particles.

The ability of $sTiO_2$ suspended in silicone oil and $ncTiO_2$ suspended in Pentalan408 to promote skin carcinogenesis was examined using the 7,12-dimethylbenz[a] anthracene (DMBA)-initiated skin carcinogenesis model employing skin carcinogenesis-sensitive animals and their wild-type counterparts as the test animals. The rasH2 mouse carries a human c-Ha-ras proto-oncogene and is highly susceptible to chemically induced skin carcinogenesis (Muto *et al.*, 2006). The Hras128 rat also carries a human c-Ha-ras proto-oncogene and highly susceptible to chemically induced skin carcinogenesis (Park *et al.*, 2004).

In addition to the animal models, we also used an *in vitro* model to examine $sTiO_2$ particle penetration into skin. Unlike animal skin, the *in vitro* model does not have hair follicles, allowing direct examination of the ability of $sTiO_2$ particles to penetrate through a layer of human skin epidermal keratinocytes.

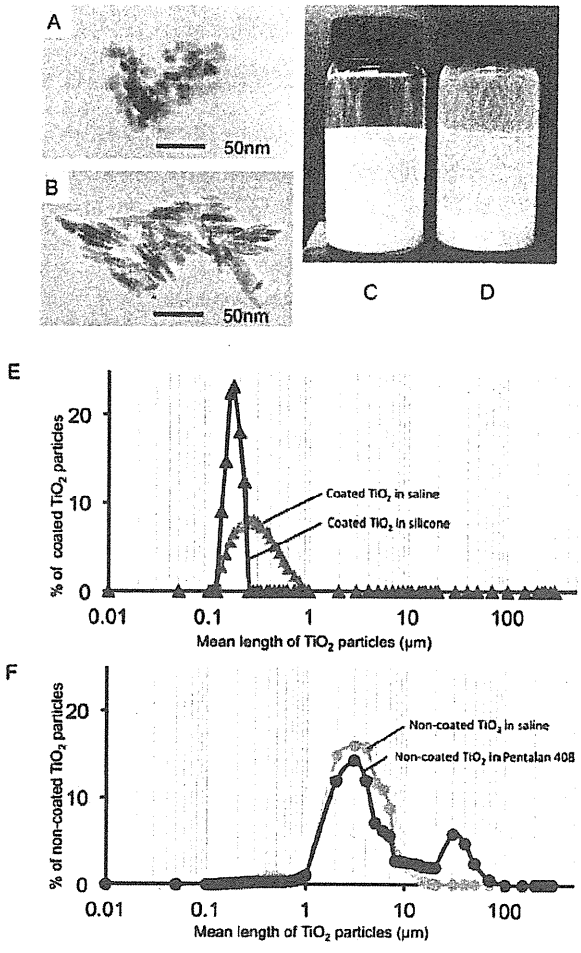

Fig. 1. Physicochemical features of $sTiO_2$ / $ncTiO_2$. $sTiO_2$ particles were round to oval in shape (A), and $ncTiO_2$ particles were club shaped (B). $sTiO_2$ particles remained evenly dispersed in silicone solution (C) while $ncTiO_2$ particles formed a white sediment at the bottom of the bottle 3 days after preparation (D). Size distribution of $sTiO_2$ suspended in saline (gray triangles) and in silicone (black triangles) (E). Size distribution of $ncTiO_2$ suspended in saline (gray circles) and in Pentalan 408 (black circles) (F). % of TiO_2 particles (Y axis) was calculated as the ratio of TiO_2 particles of a particular mean length/total particles examined.

Table 1. TiO_2 materials and animal strains used in this study

Coating status of TiO_2	Size	Concentrartion of TiO_2 (mg/ml)	Suspended in	Skin assay (Carcinogen) Strain (or *in vitro* system)
Coated (rutile type)	35 nm	50, 100	Silicone	Carcinogenesis (DMBA) rasH2 mouse, C57BL mouse
		100, 200	Silicone	Penetration LabCyte EPI-MODEL
Non-coated (rutile type)	20 nm	100, 200	Pentalan 408	Carcinogenesis (DMBA) Hras128 rat, Sprague-Dawley rat
		50, 100	Pentalan 408	Carcinogenesis (DMBA) CD1 mouse
		200	Pentalan 408	Penetration Sprague-Dawley rat

MATERIALS AND METHODS

Animals

Male rasH2 mice and Hras128 rats, known to be highly sensitive to chemically induced skin carcinogenesis (Muto *et al.*, 2006; Park *et al.*, 2004), and their wild-type counterparts, CB6F1 mice and SD rats, were purchased from CLEA Japan Co., Ltd. (Tokyo, Japan). To confirm the results, CD-1 mice, which are frequently used in skin carcinogenesis studies, were also included in this series of studies. The animals were housed in the animal center of Nagoya City University Medical School, maintained on a 12 hr light-dark cycle and received Oriental MF basal diet (Oriental Yeast Co., Tokyo, Japan) and water *ad libitum*. All animals were kept for 1 week for acclimation. The experiments were conducted according to the Guidelines for the Care and Use of Laboratory Animals, and the study protocol was approved by the Institutional Animal Care and Use Committee of Nagoya City University Medical School.

Preparation of suspensions of titanium dioxide (TiO_2) and size analysis

$sTiO_2$ particles (silicone coated, mean manufacturer's particulate diameter of 35 nm) and $ncTiO_2$ particles (rutile type, mean manufacturer's particulate diameter of 20 nm) were provided by Japan Cosmetic Association, Tokyo, Japan. Size, coating, dose and suspension vehicles and animals used are summarized in Table 1. The size distribution of $sTiO_2$ suspended in silicone oil (cyclopentasiloxane, KF-995, Shin-Etsu Chemicals Co., Tokyo, Japan) or in saline and $ncTiO_2$ particles suspended in Pentalan 408 (pentaerythritol tetraethylhexanoate, CAS7299-99-2, Nikko Chemicals Co., Tokyo, Japan) or in saline was determined by a Particle Size Distribution Analyzer (Shimadzu Techno-Research Inc., Kyoto, Japan). The shape of suspended $sTiO_2$ and $ncTiO_2$ was observed by transmission electron microscopy (JEOL Co. Ltd., Tokyo, Japan). Freshly made suspensions were sonicated for 30 min, and suspensions were sonicated again for 30 min just prior to use.

Experimental design

Skin carcinogenesis study of silicone coated TiO_2 ($sTiO_2$) using rasH2 mice

The back skin of 7-week-old female rasH2 mice (60 mice) and wild-type CB6F1 mice (60 mice) was shaved (2 × 2 cm area) and the animals received a single topical application (painting) of 0.1 ml DMBA solution (2 mg/ml in acetone). Two weeks later, the animals were divided into 3 groups and the area which was painted with DMBA was shaved and painted with silicon oil alone or $sTiO_2$ suspended in silicon oil 5 times a week until termination of the experiment: Group 1 mice (15 mice of each strain) were painted with 0.2 ml silicone oil; group 2 mice (15 mice of each strain) were painted with 0.2 ml of 50 mg/ml $sTiO_2$ suspended in silicone oil; group 3 mice (15 mice of each strain) were painted with 0.2 ml of 100 mg/ml $sTiO_2$ suspended in silicone oil. Group 4 consisted of 15 mice of each strain painted with 0.2 ml 100 mg/ml $sTiO_2$ suspended in silicon oil 5 times a week without prior DMBA treatment. The rasH2 mice were killed at experimental week 8 and wild-type CB6F1 mice were killed at experimental week 40.

Skin carcinogenesis study of non-coated TiO_2 ($ncTiO_2$) using Hras128 rats

The back skin of 10-week-old male Hras128 rats (50 rats) and wild-type SD rats (36 rats) was shaved (3 × 3 cm area) and the animals received a single topical application (painting) of 0.5 ml DMBA solution (5 mg/ml in acetone)

(Park *et al.*, 2004). Two weeks later, the animals were divided into 3 groups and the area which was painted with DMBA was shaved and painted with Pentalan 408 alone or $ncTiO_2$ suspended in Pentalan 408 twice a week until termination of the experiment: Group 1 rats (17 Hras128 and 12 SD rats) were painted with 0.5 ml Pentalan 408 alone; group 2 rats (16 Hras128 and 12 SD rats) were painted with 0.5 ml of 100 mg/ml $ncTiO_2$ suspended in Pentalan 408; group 3 rats (17 Hras128 and 12 SD rats) were painted with 0.5 ml of 200 mg/ml $sTiO_2$ suspended in Pentalan 408. The Hras128 rats were killed at experimental week 28 and wild-type SD rats were killed at experimental week 40.

Skin carcinogenesis study of non-coated TiO_2 ($ncTiO_2$) using wild-type CD1 mice

The back skin of 10-week-old female CD1 mice (62 mice) was shaved (2 × 2 cm area) and the animals received a single topical application (painting) of 0.1 ml DMBA solution (2 mg/ml in acetone). Two weeks later, the animals were divided into 4 groups and the area which was painted with DMBA was shaved and painted with Pentalan 408 alone twice a week, $ncTiO_2$ suspended in Pentalan 408 twice a week, or TPA 4 times a week (positive control) until termination of the experiment: Group 1 mice (16 mice) were painted with 0.2 ml Pentalan 408; group 2 mice (16 mice) were painted with 0.2 ml of 50 mg/ml $ncTiO_2$ suspended in Pentalan 408; group 3 mice (15 mice) were painted with 0.2 ml of 100 mg/ml $ncTiO_2$ suspended Pentalan 408; group 4 mice (15 mice) were painted with 0.2 ml TPA solution (200 nmol/ml in acetone). Group 1-3 mice were killed at experimental week 52; group 4 mice were killed at experimental week 40.

Skin penetration study of non-coated TiO_2 ($ncTiO_2$) in SD rats

Based on our previous study showing lack of TiO_2 penetration through the normal skin (Xu *et al.*, 2011), $ncTiO_2$ was applied to damaged skin, which is postulated to be more susceptible to particle penetration. The back skin of 10-week-old female SD rats (24 rats) was shaved (3 × 3 cm area) and the epidermis was removed by stripping the epidermis off with a fresh piece of adhesive tape (3M's No. 3760, Scotch Mending Tape, Sumitomo 3M Ltd., Tokyo, Japan): Stripping was done 30 times to completely remove the epidermis. The epidermis-stripped skin was then painted with 0.5 ml of Pentalan or 0.5 ml of 200 mg/ml $ncTiO_2$ suspended in Pentalan 408 at 4-day-intervals over the course of 3 and a half weeks (7 treatments in 3½ weeks). Localization of $ncTiO_2$ particles in the epidermis was determined by histological observation. Skin tissue samples were taken at 1, 3, and 7 days after stripping to examine recovery of the epidermis and penetration of $ncTiO_2$ into the skin.

Skin penetration study of silicone coated TiO_2 ($sTiO_2$) in the in vitro skin model

To evaluate whether optimally dispersed $sTiO_2$ particles could penetrate into the epidermis, we applied $sTiO_2$ particles dispersed in silicone oil to the LabCyte EPI-MODEL kit (Japan Tissue Engineering Co. Ltd., Aichi, Japan), which is constructed of human skin epidermis keratinocytes on a mesh over a receiving chamber. In 12 wells: 4 wells had silicone oil alone applied directly to the human skin epidermis keratinocytes for 48 hr; 4 wells had 100 mg/ml $sTiO_2$ suspended in silicone oil applied directly to the human skin epidermis keratinocytes for 48 hr; and 4 wells had 200 mg/ml $sTiO_2$ suspended in silicone oil applied directly to the human skin epidermis keratinocytes for 48 hr. The medium in the receiving chamber was collected for elemental titanium analysis by an inductively coupled plasma/mass spectrometry (ICP-MS) (HP-4500, Hewlett-Packard Co., Houston,TX, USA) as described previously (Xu *et al.*, 2011).

Statistical analysis

Statistical analysis was performed using the Kruskal-Wallis and Bonferroni-Dunn's multiple comparison tests. Statistical significance was analyzed using a two-tailed Student's *t*-test and Bonferroni-Dunn's multiple comparison test. A value of $P < 0.05$ was considered to be significant.

RESULTS

Size distribution of $ncTiO_2$ and $sTiO_2$ particles

Transmission electron microscopy (TEM) analysis showed that the shape of $sTiO_2$ particles was generally round to oval (Fig. 1A), while $ncTiO_2$ particles were more clubbed shaped (Fig. 1B). The $sTiO_2$ in silicone oil solutions remained without obvious sedimentation for 3 days after preparation (Fig. 1C). In contrast, the $ncTiO_2$ in Pentalan 408 solutions contained considerable sedimentation 3 days after preparation (Fig. 1D). The particle size distribution of $sTiO_2$ and $ncTiO_2$ solutions is shown in Figs. 1E and 1F. The mean length of $sTiO_2$ particles suspended in saline and silicone was 0.16 ± 0.07 and 0.28 ± 0.22 μm, respectively (Fig. 1E). The mean length of $ncTiO_2$ particles suspended in saline and Pentalan 408 was 3.18 ± 0.35 and 4.97 ± 0.50 μm, respectively (Fig. 1F). These results indicate that $sTiO_2$ in silicone oil remained dispersed for a longer time than $ncTiO_2$ in Pentalan 408.

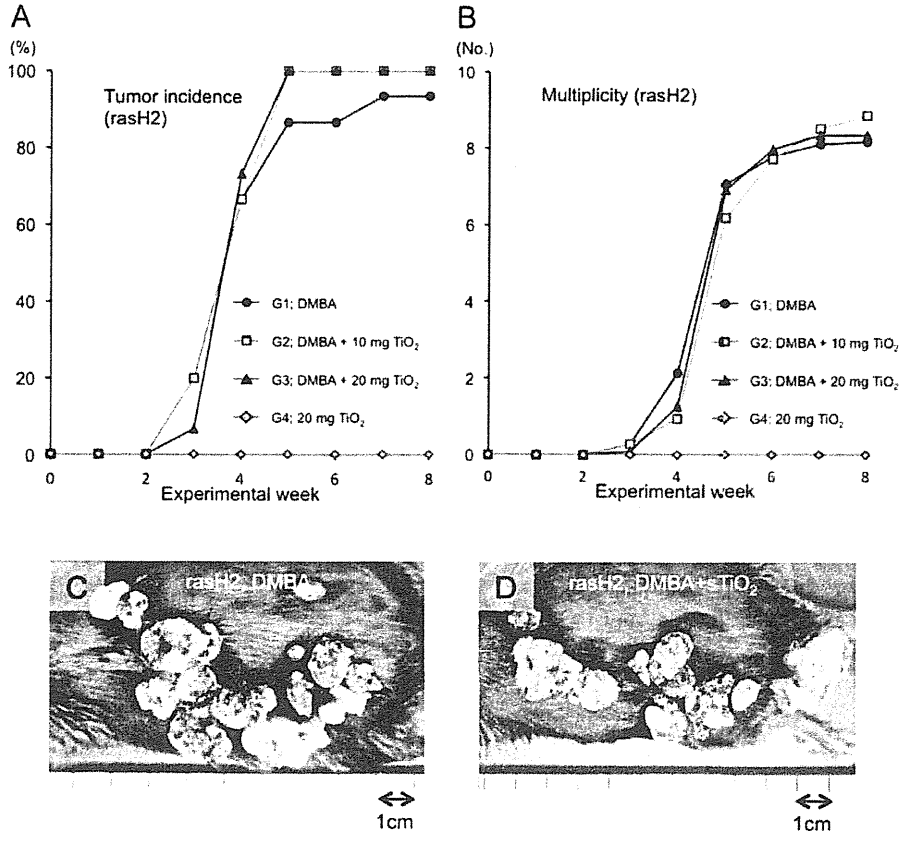

Fig. 2. Effects of $sTiO_2$ in a two-stage carcinogenesis model using rasH2 mice. The incidence of skin tumors in rasH2 mice: DMBA treated group (black circles), DMBA followed by treatment with 10 mg $sTiO_2$ (gray squares) or 20 mg $sTiO_2$ (black triangles). 20 mg $sTiO_2$ treated group (gray diamonds) (A). Multiplicity of skin tumors in rasH2 mice: DMBA treated group (black circles), DMBA followed by treatment with 10 mg $sTiO_2$ (gray squares) or 20 mg $sTiO_2$ (black triangles). 20 mg $sTiO_2$ treated group (gray diamonds) (B). Representative macroscopic appearance of skin tumors initiated with DMBA in rasH2 mice (C). The gross morphology of the tumors did not show obvious differences between the DMBA (C) and DMBA + $sTiO_2$ (D) groups.

Skin carcinogenesis study of $sTiO_2$ in silicone oil using rasH2 mice

Figures 2A and 2B show the time lapse incidence and multiplicity (number/mouse) of macroscopic skin tumors in rasH2 mice. No statistically significant differences were found between $sTiO_2$ treated rasH2 mice (groups 2 and 3: DMBA plus 50 mg/ml and 100 mg/ml $sTiO_2$, respectively) and control rasH2 mice (group 1: DMBA alone) (Figs. 2A and 2B, Table 2-1). Similarly, no statistically significant differences were found between treated and control groups of wild-type CB6F1 mice (Table 2-2). No tumors were induced in group 4 ($sTiO_2$ alone) of either rasH2 (Figs. 2A and 2B, Table 2-1) or wild-type CB6F1 mice (Table 2-2). Skin tumors were histologically SCP and SCC in rasH2 and wild-type CB6F1 mice. Representative macroscopic skin tumors induced by DMBA alone and by DMBA plus $sTiO_2$ are shown in Fig. 2C and 2D, respectively.

Skin carcinogenesis study of $ncTiO_2$ using Hras128 rat

Figures 3A and 3B show the time lapse incidence and multiplicity (number/rat) of macroscopic skin tumors in Hras128 rats. No statistically significant differences were found between $sTiO_2$ treated and control rasH2 rats (Figs. 3A and 3B, Table 3-1). Similarly, no statistically significant differences were found between treated and control groups of wild-type SD rats (Table 3-2).

Microscopically, TiO_2 was not observed within the SCP or SCC tissue (Figs. 4A and 4B). TiO_2 was observed

Table 2-1. Effects of $sTiO_2$ on skin carcinogenesis in rasH2 mice

Group	Treatment	No. of mice	SCP		SCC		SCP + SCC	
			Incidence (%)	Multiplicity	Incidence (%)	Multiplicity	Incidence (%)	Multiplicity
1	DMBA + Silicone	15	14 (93)	7.27 ± 4.74	5 (33)	0.60 ± 0.99	14 (93)	7.87 ± 5.17
2	DMBA + 10 mg TiO_2	15	15 (100)	8.13 ± 3.66	9 (60)	1.00 ± 1.00	15 (100)	9.13 ± 3.76
3	DMBA + 20 mg TiO_2	15	15 (100)	6.80 ± 3.88	8 (53)	0.73 ± 0.80	15 (100)	7.53 ± 3.31
4	20 mg TiO_2	15	0	0	0	0	0	0

SCP, squamous cell papilloma; SCC, squamous cell carcinoma.
Multiplicity: number of tumors per mouse.

Table 2-2. Effects of $sTiO_2$ on skin carcinogenesis in wild-type CB6F1 mice

Group	Treatment	No. of mice	SCP		SCC		SCP + SCC	
			Incidence (%)	Multiplicity	Incidence (%)	Multiplicity	Incidence (%)	Multiplicity
1	DMBA + Silicone	15	1 (7)	0.07 ± 0.26	1 (7)	0.07 ± 0.26	2 (13)	0.13 ± 0.35
2	DMBA + 10 mg TiO_2	15	2 (13)	0.13 ± 0.35	0	0	2 (13)	0.13 ± 0.35
3	DMBA + 20 mg TiO_2	15	2 (13)	0.20 ± 0.56	0	0	2 (13)	0.20 ± 0.56
4	20 mg TiO_2	15	0	0	0	0	0	0

SCP, squamous cell papilloma; SCC, squamous cell carcinoma.
Multiplicity: number of tumors per mouse.

on the surface and in the upper SC tissue and upper part of the hair follicles, but not in the underlying epidermis, dermis or subcutaneous tissues (Figs. 4C and 4D).

Skin carcinogenesis study of $ncTiO_2$ using wild-type CD1 mice

No statistically significant differences in tumor incidence or multiplicity was observed between treated and control groups of CD1 mice (Table 4). TPA treatment after DMBA significantly increased the incidence and multiplicity of SCP ($P < 0.001$).

Skin penetration study of $ncTiO_2$ in SD rats

Figures 5 A-D shows skin tissue samples collected before (Fig. 5A) and 1, 3 and 7 days after (Figs. 5B-D) removing the epidermis by tape-stripping. On day 1 the epidermis was completely removed (Fig. 5B), and a mass of fibrin exudate and underlying granulation tissue rich with neutrophils was the main feature of the skin surface. On day 3, regenerated epidermis already covered the granulation tissue (Fig. 5C). On day 7, the surface of the skin was fully covered by regenerated keratinocytes showing cornification and had an almost normal appearance (Fig. 5D).

The shaved back skin of SD-rats was painted with 100 mg TiO_2 suspended in Pentalan 408. Fig. 5E shows the presence of $ncTiO_2$ particles in the SC layer of the skin of these animals. Extensive histological observation failed to detect TiO_2 within the epidermis or dermis. In another series of experiments, the epidermis was removed from the back skin of SD rats by tape-stripping and the freshly stripped skin was painted with 100 mg $ncTiO_2$ suspended in Pentalan 408. This was repeated every 4 days for 3½ weeks (7 times total). Figure 5F shows the presence of TiO_2 on the surface of the regenerating epidermis 1 day after the last stripping/painting procedure. Extensive

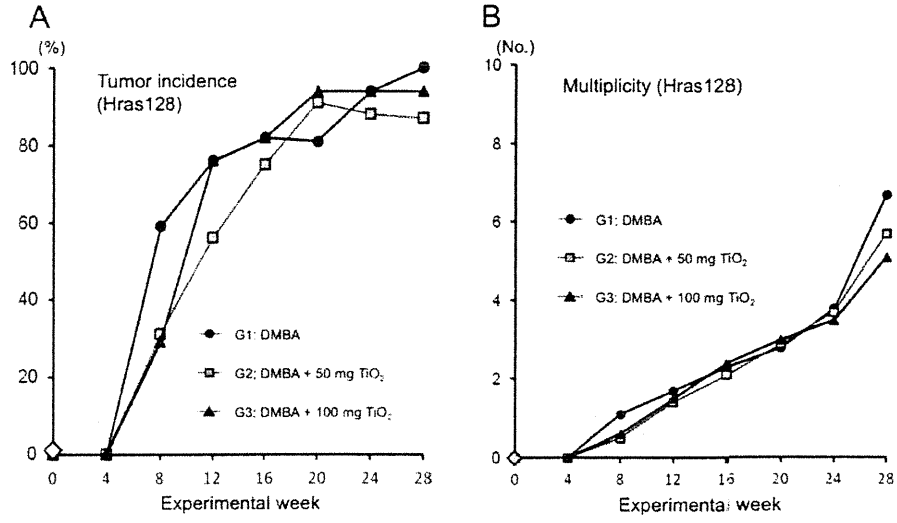

Fig. 3. Effects of $ncTiO_2$ in a two-stage carcinogenesis model using Hras128 rats. The incidence of skin tumors in Hras128 rats: DMBA treated group (black circles), DMBA followed by treatment with 50 mg $ncTiO_2$ (gray squares) or 100 mg $ncTiO_2$ (black triangles) (A). Multiplicity of skin tumors in rasH2 mice: DMBA treated group (black circles), DMBA followed by treatment with 100 mg $ncTiO_2$ (gray squares) or 200 mg $ncTiO_2$ (black triangles) (B).

Table 3-1. Effects of $ncTiO_2$ on skin carcinogenesis in Hras128 rats

Group	Treatment	No. of rats	SCP		SCC		SCP + SCC	
			Incidence (%)	Multiplicity	Incidence (%)	Multiplicity	Incidence (%)	Multiplicity
1	DMBA + Pentalan 408	17	16 (94)	9.65 ± 7.05	0	0	16 (94)	9.65 ± 7.05
2	DMBA + 50 mg TiO_2	16	14 (88)	6.81 ± 6.21	2 (13)	0.19 ± 0.54	14 (88)	7.00 ± 6.52
3	DMBA + 100 mg TiO_2	17	16 (94)	7.59 ± 3.86	2 (12)	0.12 ± 0.331	16 (94)	7.71 ± 3.93

SCP, squamous cell papilloma; SCC, squamous cell carcinoma.
Multiplicity: number of tumors per rat.

Table 3-2. Effects of $ncTiO_2$ on skin carcinogenesis in wild-type SD rats

Group	Treatment	No. of rats	SCP		SCC		SCP + SCC	
			Incidence (%)	Multiplicity	Incidence (%)	Multiplicity	Incidence (%)	Multiplicity
1	DMBA + Pentalan 408	12	3 (25)	0.25 ± 0.45	0	0	3 (25)	0.25 ± 0.45
2	DMBA + 50 mg TiO_2	12	2 (17)	0.17 ± 0.39	2 (17)	0.17 ± 0.39	4 (33)	0.33 ± 0.49
3	DMBA + 100 mg TiO_2	12	1 (8)	0.08 ± 0.29	0	0	1 (8)	0.08 ± 0.29

SCP, squamous cell papilloma; SCC, squamous cell carcinoma.
Multiplicity: number of tumors per rat.

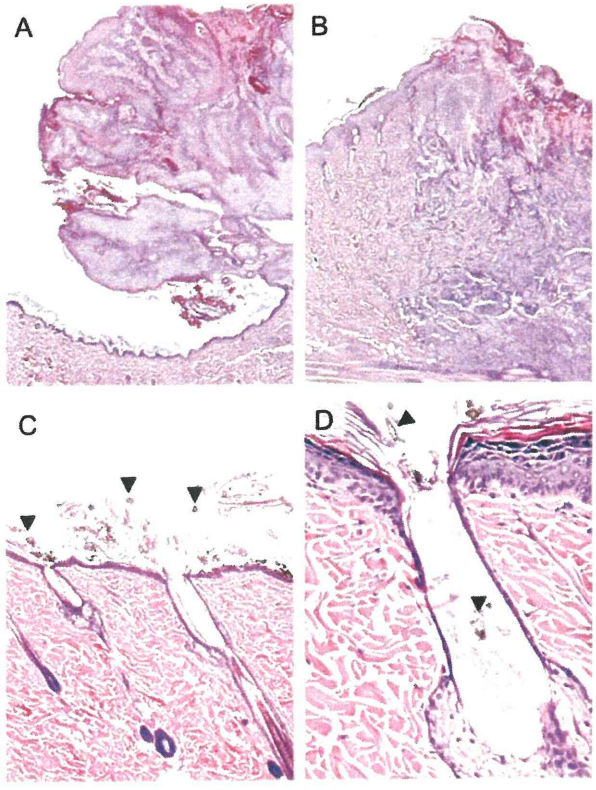

Fig. 4. Effects of $ncTiO_2$ in a two-stage carcinogenesis model. Representative histological features of SCP (A) and SCC (B) on the back skin of a Hras128 rat. TiO_2 aggregates were seen on the surface of stratum corneum (C, arrowheads), but not in the underlying epidermis, dermis or subcutaneous tissue. Some aggregates were found in the upper layer of stratum corneum (arrowheads) and in the lumen of the hair follicle (D) but not in the dermis.

histological observation failed to detect any TiO_2 particles in the underlying epidermis or dermis, indicating that $ncTiO_2$ failed to penetrate into the stripped skin. In addition, no inflammatory lesions were found in the epidermis or subcutaneous tissue of these animals. These results indicate that TiO_2 particles do not penetrate into the epidermis of either normal or damaged skin.

In vitro skin penetration study

The amount of elemental titanium in the receiving chamber did not show any significant increase over the vehicle group (Table 5). All the observed values are equivalent to background. The results indicate that $sTiO_2$ particles did not penetrate the human epidermis in this model.

DISCUSSION

TiO_2 particles, including both nano and larger sized particles, are known to be carcinogenic to the rat lung (Baan *et al.*, 2006). We have shown that alveolar macrophages play an important role in promotion of lung carcinogenesis when TiO_2 particles are inhaled into the lung (Xu *et al.*, 2011). Because of this, TiO_2 particles, especially nano-sized particles, are deemed to have the potential to induce skin tumors after long-term topical application should the particles penetrate into the epidermis and subcutaneous tissue and interact with macrophages. The current study is the first systematic study of the skin promotion/carcinogenesis effects of TiO_2 in a two-stage chemical carcinogenesis animal model. We found that even the smallest available sized TiO_2 ($sTiO_2$) did not exhibit promoting effects on the highly sensitive rasH2 mouse skin carcinogenesis model. Furthermore, we observed that TiO_2 without coating ($ncTiO_2$) did not cause skin tumor promotion in the skin carcinogenesis-sensitive Hras128 rat model or in the CD1 mouse. These results are in agreement with another recent study reporting the lack of carcinogenicity of topically applied TiO_2 (Furukawa *et al.*, 2011).

We also found that topically applied $ncTiO_2$ did not penetrate normal rat skin or skin which had the epidermis completely removed, nor did $sTiO_2$ penetrate the *in vitro* human epidermis model. Thus, the lack of skin promotion/carcinogenesis effects is probably due to lack of penetration of the particles through the epidermis to the dermis where cytogenetic cells of skin carcinogenesis reside. In another study, we found no promoting effect of TiO_2 particles in a UVB-initiated long-term (52 weeks) skin carcinogenesis study and no penetration of TiO_2 particles through the epidermis (Xu *et al.*, 2011).

Results showing lack of TiO_2 penetration through the epidermis are in accordance with other reports. Numerous *in vitro* and *in vivo* studies using murine, porcine, or human skin have shown that nano-sized TiO_2 does not penetrate the skin (reviewed in Nohynek *et al.* (2008)). In addition to these studies, Gottbrath *et al.* (2003) report that after topical application of TiO_2 to the underside of the forearm of a human volunteer, ultrafine TiO_2 did not penetrate beyond the SC.

Contrary to these findings, there is a single report by Wu *et al.* (2009) that TiO_2 particles (4 and 60 nm) did penetrate into the deep layers of the epidermis after topical application to the pig ear for 30 days (Wu *et al.*, 2009). They also reported that nano-size TiO_2 particles could penetrate the skin of hairless mice after 60 days dermal exposure, although they did not examine promotion/car-

Table 4. Effects of $ncTiO_2$ on skin carcinogenesis in wild-type CD1 mice

Group	Treatment	No. of mice	SCP		SCC		SCP + SCC	
			Incidence (%)	Multiplicity	Incidence (%)	Multiplicity	Incidence (%)	Multiplicity
1	DMBA + Pentalan 408	16	3 (19)	0.25 ± 1.30	0	0	3 (19)	0.25 ± 0.58
2	DMBA + 10 mg TiO_2	16	1 (6)	0.06 ± 0.25	0	0	1 (6)	0.06 ± 0.25
3	DMBA + 20 mg TiO_2	15	2 (13)	0.13 ± 0.35	0	0	2 (13)	0.13 ± 0.35
4	DMBA + TPA	15	13 (87)*	2.00 ± 1.41*	2 (13)	0.13 ± 0.35	13 (87)*	2.00 ± 1.41*

* Significantly different from group 1 (control) by Student's t-test ($p < 0.001$).
SCP, squamous cell papilloma; SCC, squamous cell carcinoma.
Multiplicity: number of tumors per mouse.

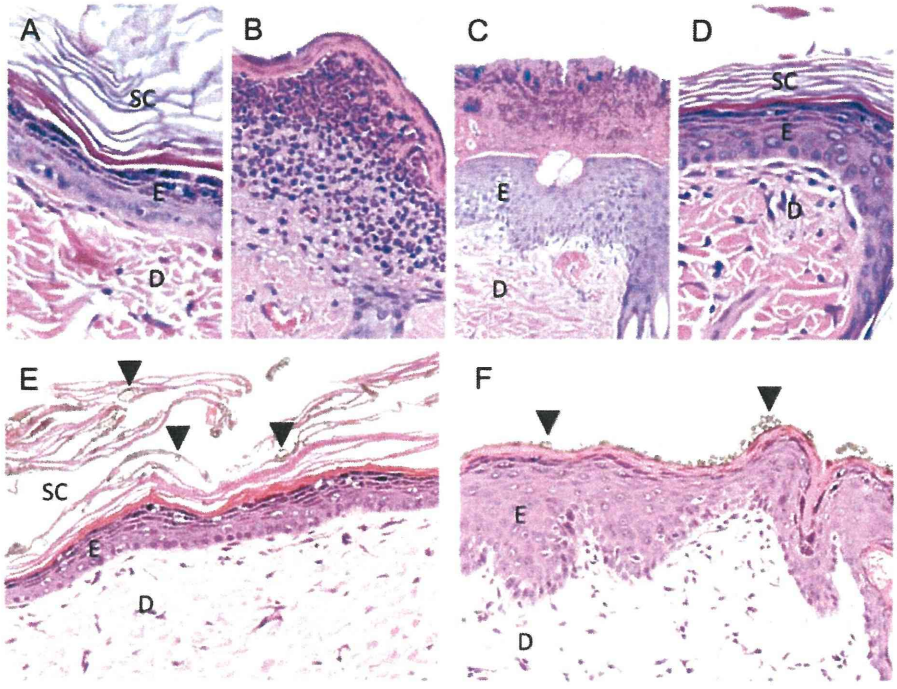

Fig. 5. Histological features of the skin after striping away the epidermis and study of $ncTiO_2$ penetration into normal and stripped skin using wild-type Sprague-Dawley rats. The back skin of SD rats was shaved and the epidermis was left intact or stripped away using tape. Stratum corneum (SC), epidermis (E), and dermis (D) are intact in the shaved, not stripped group (A). In the tape-stripped group, one day after stripping away the epidermis, the stripping site is covered with fibrin exudates with rich neutrophilic infiltration (B). Three days after stripping, regenerated epidermis (E) is present underneath the exudate (C). Seven days after stripping, the regenerated epidermis (E) is composed of mature keratinocytes and a stratum corneum (SC) (D). The back skin of SD rats was shaved (but the epidermis was not stripped away) and painted with $ncTiO_2$ suspended in Pentalan 408. $ncTiO_2$ aggregates are present in the stratum corneum (SC) (arrowheads, brown material) of the skin of these animals (E); particles were not detected within the underlying skin tissue. Freshly stripped skin was painted with $ncTiO_2$ suspended in Pentalan 408, and this process was repeated every 4 days over the course of $3^1/_2$ weeks (7 times total). $ncTiO_2$ particles (arrowheads, brown material) are present on the surface of the skin one day after the last stripping/painting procedure (F); particles were not detected in the underlying tissue.

Table 5. *In vitro* penetration of $sTiO_2$ particles

Treatment	Amount of elemental titanium in the receiving chamber (μg/ml)
Silicone oil	0.11 ± 0.01
100 mg/ml $sTiO_2$	0.14 ± 0.01
200 mg/ml $sTiO_2$	0.12 ± 0.01
None	0.11 ± 0.03

cinogenesis effects of the particles (Wu *et al.*, 2009). Differences in experimental systems (i.e., animal strain used in the experiment, exposure period, particle suspension, mean primary/actual length of the particle, and TiO_2 manufacturer) may possibly explain the discrepancies reported on TiO_2 particle penetration.

Two studies have reported finding TiO_2 particles in hair follicles (Bennat and Muller-Goymann, 2000; Lekki *et al.*, 2007). These studies taken together with Wu *et al.* (2009) suggest the possibility that the hair follicle may be a route of skin penetration by TiO_2 particles. However, we found that TiO_2 particles remained primarily in the SC and the upper lumen of hair follicles. Bennat and Muller-Goymann (2000) and Lekki *et al.* (2007) also report that while topically applied TiO_2 was found in hair follicules, it did not penetrate into the underlying tissue or sebaceous glands.

Penetration of TiO_2 into underlying dermal tissues even after removing the entire epidermis by tape-stripping did not occur. Rather, aggregates of TiO_2 particles were found on the exterior of the SC exhibiting regeneration and no particles were found in the underlying tissues. The freshly manufactured TiO_2 particles used in the present study primarily measured 20-35 nm in their longer diameter. These particles are lyophobic and easily form micro-sized aggregates (160-5,000 nm in length), and these larger particles are unable to penetrate through the epidermis.

In summary, nano-sized TiO_2 particles, even silicone coated TiO_2 suspended in silicone oil which provides optimal dispersion of the particles, did not penetrate the epidermis of rat or human skin models and did not exhibit promoting effects in rat or mouse two-stage skin carcinogenesis models. Therefore, topical application of TiO_2 was not carcinogenic, and this lack of carcinogenicity is likely due to the lack of penetration through the epidermis. Our studies taken together with other reports lead us to conclude that topical application of TiO_2 to human skin is very unlikely to pose a potential risk to human health.

ACKNOWLEDGMENTS

This work was supported by Health and Labour Sciences Research Grants (Research on Risk of Chemical Substance, H19-kagaku-ippan-006 and H22-kagaku-ippan-005), and Grant-in aid for cancer research from the Ministry of Health, Labour and Welfare, Japan.

REFERENCES

Baan, R., Straif, K., Grosse, Y., Secretan, B., El Ghissassi, F. and Cogliano, V. (2006): Carcinogenicity of carbon black, titanium dioxide, and talc. Lancet Oncol., **7**, 295-296.

Baan, R.A. (2007): Carcinogenic hazards from inhaled carbon black, titanium dioxide, and talc not containing asbestos or asbestiform fibers: recent evaluations by an IARC Monographs Working Group. Inhal. Toxicol., **19**, 213-228.

Bennat, C. and Muller-Goymann, C.C. (2000): Skin penetration and stabilization of formulations containing microfine titanium dioxide as physical UV filter. Int. J. Cosmet. Sci., **22**, 271-283.

Furukawa, F., Doi, Y., Suguro, M., Morita, O., Kuwahara, H., Masunaga, T., Hatakeyama, Y. and Mori, F. (2011): Lack of skin carcinogenicity of topically applied titanium dioxide nanoparticles in the mouse. Food Chem. Toxicol., **49**, 744-749.

Gelis, C., Girard, S., Mavon, A., Delverdier, M., Paillous, N. and Vicendo, P. (2003): Assessment of the skin photoprotective capacities of an organo-mineral broad-spectrum sunblock on two ex vivo skin models. Photodermatol. Photoimmunol. Photomed., **19**, 242-253.

Gottbrath, S, C.M.-G. (2003): Penetration and visualization of titanium dioxide microparticles in human stratum corneum-effect of different formulations on the penetration of titanium dioxide. SOFW Journal, **129**, 11-17.

Lekki, J., Stachura, Z., Dąbroś, W., Stachura, J., Menzel, F., Reinert, T., Butz, T., Pallon, J.. Gontier, E., Ynsa, M.D., Moretto, P., Kertesz, Z., Szikszai, Z. and Kiss, A.Z. (2007): On the follicular pathway of percutaneous uptake of nanoparticles: Ion microscopy and autoradiography studies. Nucl. Instrum. Methods Phys. Res., Section B, **260**, 174-177.

Muto, S., Katsuki, M. and Horie, S. (2006): Rapid induction of skin tumors in human but not mouse c-Ha-ras proto-oncogene transgenic mice by chemical carcinogenesis. Cancer Sci., **97**, 842-847.

Newman, M.D., Stotland, M. and Ellis, J.I. (2009): The safety of nanosized particles in titanium dioxide- and zinc oxide-based sunscreens. J. Am. Acad. Dermatol., **61**, 685-692.

Nohynek, G.J., Dufour, E.K. and Roberts, M.S., (2008): Nanotechnology, cosmetics and the skin: is there a health risk? Skin. Pharmacol. Physiol., **21**, 136-149.

Park, C.B., Fukamachi, K., Takasuka, N., Han, B.S., Kim, C.K., Hamaguchi, T., Fujita, K., Ueda, S. and Tsuda, H. (2004): Rapid induction of skin and mammary tumors in human c-Ha-ras proto-oncogene transgenic rats by treatment with 7,12-dimethylbenz[a] anthracene followed by 12-O-tetradecanoylphorbol 13-acetate. Cancer Sci., **95**, 205-210.

Rouabhia, M., Mitchell, D.L., Rhainds, M., Claveau, J. and Drouin, R. (2002): A physical sunscreen protects engineered human skin against artificial solar ultraviolet radiation-induced tissue and DNA damage. Photochem. Photobiol. Sci., **1**, 471-477.

Schaefer, H., Redelmaier, T. and Nohynek, G. (2003): Pharmacok-

inetics and topical application of drugs. In Fitzpatrick's Dermatology in General Medicine (Freedberg, I., Eisen, A., Wolff, K., Austen, F., Goldsmith, L. and Katz, S. eds.), pp.2313-2318, McGraw-Hill, New York.

Senzui, M., Tamura, T., Miura, K., Ikarashi, Y., Watanabe, Y. and Fujii, M. (2010): Study on penetration of titanium dioxide (TiO(2)) nanoparticles into intact and damaged skin in vitro. J. Toxicol. Sci., **35**, 107-113.

Suzuki, M. (1987): Protective effect of fine-particle titanium dioxide on UVB-induced DNA damage in hairless mouse skin. Photodermatol., **4**, 209-211.

Wu, J., Liu, W., Xue, C., Zhou, S., Lan, F., Bi, L., Xu, H., Yang, X. and Zeng, F.D. (2009): Toxicity and penetration of TiO2 nanoparticles in hairless mice and porcine skin after subchronic dermal exposure. Toxicol. Lett., **191**, 1-8.

Xu, J., Sagawa, Y., Futakuchi, M., Fukamachi, K., Alexander, D.B., Furukawa, F., Ikarashi, Y., Uchino, T., Nishimura, T., Morita, A., Suzui, M. and Tsuda, H. (2011): Lack of promoting effect of titanium dioxide particles on ultraviolet B-initiated skin carcinogenesis in rats. Food Chem. Toxicol., **49**, 1298-1302.

Xu, J., Futakuchi, M., Iigo, M., Fukamachi, K., Alexander, DB., Shimizu, H., Sakai, Y., Tamano, S., Furukawa, F., Uchino, T., Tokunaga, H., Nishimura, T., Hirose, A., Kanno, J. and Tsuda, H. (2010): Involvement of macrophage inflammatory protein 1alpha (MIP1alpha) in promotion of rat lung and mammary carcinogenic activity of nanoscale titanium dioxide particles administered by intra-pulmonary spraying. Carcinogenesis, **31**, 927-935.

nature genetics

Mutations in *UVSSA* cause UV-sensitive syndrome and destabilize ERCC6 in transcription-coupled DNA repair

Xue Zhang[1,6], Katsuyoshi Horibata[1,2,6], Masafumi Saijo[1,6], Chie Ishigami[1], Akiko Ukai[2], Shin-ichiro Kanno[3], Hidetoshi Tahara[4], Edward G Neilan[5], Masamitsu Honma[2], Takehiko Nohmi[2], Akira Yasui[3] & Kiyoji Tanaka[1]

UV-sensitive syndrome (UV^SS) is an autosomal recessive disorder characterized by photosensitivity and deficiency in transcription-coupled repair (TCR), a subpathway of nucleotide-excision repair that rapidly removes transcription-blocking DNA damage[1]. Cockayne syndrome is a related disorder with defective TCR and consists of two complementation groups, Cockayne syndrome (CS)-A and CS-B, which are caused by mutations in *ERCC8* (*CSA*) and *ERCC6* (*CSB*), respectively[2]. UV^SS comprises three groups, UV^SS/CS-A, UV^SS/CS-B and UV^SS-A, caused by mutations in *ERCC8*, *ERCC6* and an unidentified gene, respectively[3–6]. Here, we report the cloning of the gene mutated in UV^SS-A by microcell-mediated chromosome transfer. The predicted human gene *UVSSA* (formerly known as *KIAA1530*)[7] corrects defective TCR in UV^SS-A cells. We identify three nonsense and frameshift *UVSSA* mutations in individuals with UV^SS-A, indicating that *UVSSA* is the causative gene for this syndrome. The UVSSA protein forms a complex with USP7 (ref. 8), stabilizes ERCC6 and restores the hypophosphorylated form of RNA polymerase II after UV irradiation.

To clone the gene responsible for UV^SS-A, mouse chromosomes were randomly transferred to Kps3 cells (UV^SS-A) by microcell-mediated chromosome transfers (MMCTs)[9] using mouse A9 cells as the donor. Kps3 cells fused with A9 microcells were UV irradiated periodically over 6 weeks. We obtained four independent UV-resistant cellular clones (15A-7, KAB1-14, KAGA2-6 and KAGB2-4) that exhibited normal levels of UV sensitivity and recovery of RNA synthesis after UV irradiation (UV-RRS) (**Supplementary Fig. 1**). To identify the mouse genomic DNA that was integrated in each clone, a comparative genomic hybridization (CGH) array analysis was performed. An intact mouse chromosome 5 was found in KAB1-14, whereas chromosome 5 with segments of chromosomes 12 and 17 was found in KAGA2-6. Only a few fragments of chromosome 5 were found in the 15A-7 and KAGB2-4 clones (**Fig. 1a**). These results indicated that the causative gene was located within the common 600-kb region of chromosome 5 that was integrated in the 15A-7 and KAGB2-4 clones (**Fig. 1b**). There are 11 known genes in that region (**Fig. 1c**). Six BAC clones[10] encompassing the 600-kb region were introduced into Kps3 cells (**Fig. 1c**). Kps3 clones transfected with BAC 476L03 acquired normal levels of UV resistance, whereas transfection with BAC 154C21 failed to complement UV-sensitive cells (**Fig. 1d**). These results indicate that *4933407H18Rik* is a complementing gene for UV^SS-A. The *4933407H18Rik* gene is the mouse homolog of a predicted human gene, *KIAA1530*, which has subsequently been renamed *UVSSA* (encoding UV-stimulated scaffold protein A) in light of this finding, with support from the Human Gene Nomenclature Committee (HGNC).

Sequencing of *UVSSA* cDNA in UV^SS-A cells revealed that Kps3 (Japanese)[4] and XP24KO (Japanese)[11] cells had a homozygous c.367A>T transversion, resulting in premature termination at amino acid 123 (p.Lys123*). TA-24 (Iranian)[3] cells had a homozygous deletion, c.87delG, that caused a frameshift at position 29, leading to premature termination at amino acid 39 (p.Ile31Phefs*9) (**Fig. 2a,b**). In addition, the expression of cDNA encoding Flag-HA-UVSSA successfully conferred normal levels of UV-RRS and UV resistance to Kps3 cells (**Fig. 2c,d**). Taken together, these results indicate that *UVSSA* is the causative gene for UV^SS-A.

The *UVSSA* gene is located on human chromosome 4 at p16.3 and is 40.7 kb long. The transcript of the gene is 4,336 nt long and is composed of 14 exons, encoding a protein that consists of 709 amino acids with a deduced molecular weight of 81 kDa[7,12]. Analysis of the amino-acid sequence of UVSSA revealed that there is a Vps27, Hrs and STAM (VHS) domain and a structurally similar epsin NH_2-terminal homology (ENTH) domain in the N-terminal region and a well-conserved domain of unknown function (DUF) 2043 domain in the C-terminal region (**Fig. 2a**). It was reported that the VHS/ENTH domains of SCAF8 and NRD1 interact with the C-terminal domain of RNA polymerase II (RNA Pol II)[13,14], suggesting that UVSSA also interacts with RNA Pol II. Homologs of UVSSA have been identified in *Arabidopsis thaliana*, rice and *Caenorhabditis elegans*, but there are no reports of their function.

To elucidate the function of UVSSA in TCR, we first examined its interaction with other TCR factors (**Fig. 3**). The UVSSA protein complex was affinity purified from the soluble or chromatin

[1]Graduate School of Frontier Biosciences, Osaka University, Osaka, Japan. [2]Division of Genetics and Mutagenesis, National Institute of Health Sciences, Tokyo, Japan. [3]Division of Dynamic Proteome, Institute of Development, Aging and Cancer, Tohoku University, Sendai, Japan. [4]Department of Cellular and Molecular Biology, Graduate School of Biomedical Sciences, Hiroshima University, Hiroshima, Japan. [5]Division of Genetics, Children's Hospital Boston, Center for Life Science Boston, Boston, Massachusetts, USA. [6]These authors contributed equally to this work. Correspondence should be addressed to K.T. (ktanaka@fbs.osaka-u.ac.jp).

Received 26 September 2011; accepted 29 February 2012; published online 1 April 2012; doi:10.1038/ng.2228

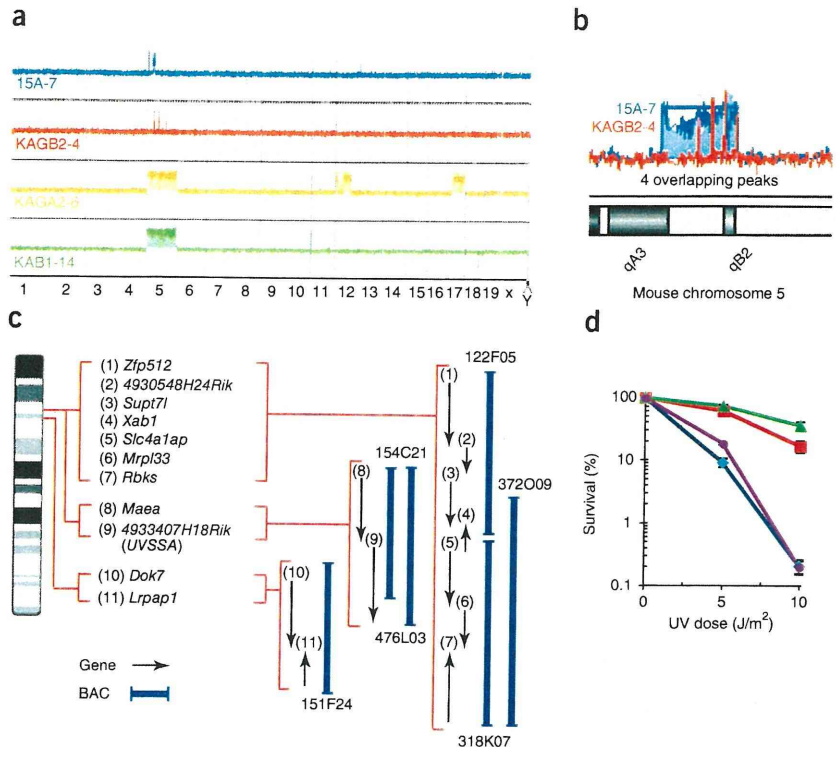

Figure 1 CGH array analysis and identification of BAC clones encompassing mouse genomic DNA integrated in the 15A-7 and KAGB2-4 clones. (**a**) CGH array analysis for identification of mouse genomic DNA integrated into the Kps3 clones containing mouse A9 chromosome segments. Kps3 cells were used as a control. (**b**) Enlarged view of the mouse chromosome 5 region integrated into the 15A-7 and KAGB2-4 clones. (**c**) Schematic of BAC clones encompassing the common 600-kb region of mouse genomic DNA integrated in clones 15A-7 and KAGB2-4. Genes included in the region are listed in positional order with a corresponding number. Chromosomal regions in red brackets correspond to peaks 2 to 4, from the left side, in **b**; there are no genes in peak 1. Arrows indicate the direction of the genes. (**d**) UV survival of Kps3 cells transfected with BAC 476L03 (green triangles) or BAC 154C21 (purple circles), compared to normal human WI38VA13 cells (red squares) and parental Kps3 cells (blue rhombuses). Error bars, s.d. calculated from three independent experiments.

fraction of extracts derived from Kps3 cells expressing Flag- and HA-tagged wild-type UVSSA. In the soluble fraction, ERCC8 was coimmunoprecipitated with UVSSA, irrespective of UV irradiation, but not with RNA Pol II or ERCC6 (**Fig. 3a**). In the chromatin fraction, ERCC6, ERCC8 and RNA Pol II were coimmunoprecipitated with UVSSA after UV irradiation (**Fig. 3b**).

Next, we searched for new TCR proteins that interact with UVSSA. The wild-type UVSSA protein fused with Flag and HA tags was stably expressed in HEK293 cells. Whole-cell extract was used for affinity purification of the UVSSA complex with antibodies to Flag and HA. Mass spectrometric analysis of the UVSSA complex identified USP7 as an interacting protein (**Supplementary Fig. 2**). USP7 is a ubiquitin-specific protease that recognizes and removes ubiquitin from proteins. Numerous proteins have been identified as potential substrates of USP7, including Mdm2, p53, claspin, Chfr and histone H2B[8,15]. To determine whether USP7 is involved in TCR, wild-type cells were treated with *USP7* small interfering RNA (siRNA) (**Fig. 3c**). *USP7* siRNA–treated cells showed decreased UV-RRS and UV survival, implicating USP7 in TCR (**Fig. 3d,e**). In the *USP7* siRNA–treated cells, not only USP7 protein levels, but also those of UVSSA, were decreased (**Figs. 3c** and **4a**). The amount of *UVSSA* mRNA was not affected in *USP7* siRNA–treated cells (**Supplementary Fig. 3**). Conversely, knockdown of *UVSSA* did not result in decreased USP7 protein levels (**Fig. 4a**), probably because of a much greater quantity of USP7 relative to UVSSA in the cells. The amount of ERCC8 protein was not affected in *USP7* siRNA–treated cells (**Fig. 4b**). These results indicate that UVSSA forms a stable complex with USP7 and transiently binds ERCC8. Also, the UVSSA-USP7 complex was coimmunoprecipitated with ERCC8, irrespective of UV irradiation in the soluble fraction, and it was coimmunoprecipitated with ERCC6, ERCC8 and RNA Pol II in the UV-damaged chromatin fraction (**Fig. 3a,b**). Coimmunoprecipitation was also detected in the cells expressing a normal level of *UVSSA* (**Supplementary Fig. 4**). These results indicate that the UVSSA-USP7 complex and ERCC8 are recruited to the sites of RNA Pol II and ERCC6 in the UV-damaged chromatin fraction. In the accompanying paper by Schwertman *et al.*, it was shown that both ERCC6 and UVSSA were recruited to the spot locally irradiated with 254-nm UV-C light, although the recruitment of ERCC6 and UVSSA was much weaker than that of the global genome-repair protein XPC[16]. These results suggest that only a small portion of cellular UVSSA is involved in TCR.

It is known that ERCC6 has an essential role in recruiting TCR factors to the stalled RNA Pol II complex[17,18]. To examine whether the binding of UVSSA, USP7 and ERCC8 to RNA Pol II is dependent on ERCC6, the Flag- and HA-tagged UVSSA protein was expressed in CS1AN (CS-B) cells, and immunoprecipitation of the cell extracts was performed using antibodies to Flag and HA. USP7 and ERCC8 were coimmunoprecipitated with UVSSA in the chromatin fraction, irrespective of UV irradiation, but RNA Pol II was not, even after UV irradiation (**Fig. 3f**). These results suggest that UVSSA, USP7 and ERCC8 are loaded onto RNA Pol II in an ERCC6-dependent manner.

Next, to examine whether the binding of UVSSA and USP7 to ERCC6 and RNA Pol II is dependent on ERCC8, the Flag- and HA-tagged UVSSA protein was expressed in CS3BE (CS-A) cells, and immunoprecipitation of the cell extracts was performed using antibodies to Flag and HA. USP7 was coimmunoprecipitated with UVSSA in the chromatin fraction, irrespective of UV irradiation, but RNA Pol II and ERCC6 were not coimmunoprecipitated, even after UV irradiation (**Fig. 3g**). These results suggest that ERCC8 is required for recruitment of the UVSSA-USP7 complex to ERCC6 and RNA Pol II in the UV-irradiated chromatin fraction. In the accompanying paper by Schwertman *et al.*, it was shown that GFP-UVSSA accumulated at sites of UV damage caused by a 266-nm UV-C laser in CS-A and CS-B cells, and a UV-independent interaction between hyperphosphorylated RNA Pol II (RNA Pol IIo) and UVSSA was detected in CS-B cells by chromatin immunoprecipitation (ChIP) using cross-linking reagent[16]. We assume that ERCC6 is required for stable integration of UVSSA, USP7, ERCC8 and RNA Pol II into a functional TCR complex.

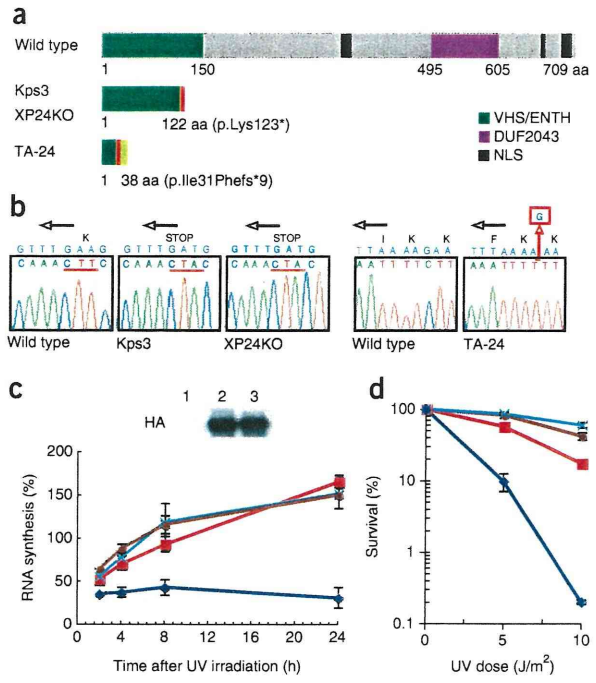

Figure 2 Mutations within the *UVSSA* gene in three subjects with UV^{S}S-A. (**a**) Schematic of the UVSSA protein and of amino-acid changes in Kps3, XP24KO and TA-24 cells. Amino-acid changes are shown in red. (**b**) Sequence chromatograms showing mutations in Kps3, XP24KO and TA-24 cells. The homozygous c.367A>T transversion is shown in Kps3 and XP24KO cells, and the homozygous c.87delG mutation is indicated in TA-24 cells. Translated amino acids are labeled above the cDNA sequence. Arrows represent the direction in which the sequence is read. (**c**) UV-RRS of Kps3 clones stably expressing *UVSSA* cDNA. Upper, protein blot of the Kps3 clones stably expressing Flag- and HA-tagged UVSSA using antibody to HA: lane 1, parental Kps3; lane 2, UVSSA-corrected Kps3 clone 1; lane 3, UVSSA-corrected Kps3 clone 2. Lower, UV-RRS of clones 1 (brown circles) and 2 (aqua crosses) and of WI38VA13 (red squares) and parental Kps3 cells (blue rhombuses). Error bars, s.d. calculated from three independent experiments. (**d**) UV survival of the Kps3 clones stably expressing Flag- and HA-tagged UVSSA. Symbols for each cell line are the same as in **c**. Error bars, s.d. calculated from three independent experiments.

We have found that the ERCC8 protein is translocated to the nuclear matrix after UV irradiation in an ERCC6- and transcription factor IIH (TFIIH)-dependent manner and that it colocalizes with Pol IIo[17,19]. Using a cell-free system[19], we found that UVSSA enhances UV-induced translocation of ERCC8 to the nuclear matrix (**Supplementary Fig. 5**).

It is known that inhibition of transcription after UV irradiation not only results from a blockage of transcription elongation by DNA damage on the transcribed strand but also can be caused by a reduction in the levels of the hypophosphorylated form of RNA polymerase II (RNA Pol IIa), which is required for the initiation of transcription[20]. The restoration of RNA Pol IIa levels and transcription after UV irradiation are deficient in CS-A and CS-B cells[20]. Consistent with this, we found that RNA Pol IIa disappeared after UV irradiation (10 J/m^2) in both the parental CS3BE (CS-A) cells and in ERCC8-corrected CS3BE cells. Approximately 16 h after UV irradiation, RNA Pol IIa reappeared in the ERCC8-corrected CS3BE cells but not in the parental CS3BE cells (**Supplementary Fig. 6**). We then examined the phosphorylation status of RNA Pol II in whole-cell lysates from Kps3 cells and UVSSA-corrected Kps3 cells after 10 J/m^2 of UV irradiation (**Fig. 4c**). RNA Pol IIa disappeared in both the parental and UVSSA-corrected Kps3 cells. However, it reappeared 8 h after UV irradiation in the UVSSA-corrected Kps3 cells but not in the parental Kps3 cells, indicating that UVSSA is required, in addition to ERCC6 and ERCC8, for the reappearance of RNA Pol IIa after UV irradiation.

Moreover, the amount of ERCC6 protein decreased in the non-irradiated parental Kps3 cells compared to the amount in the UVSSA-corrected Kps3 cells, and a greater decrease was detected after UV irradiation in the parental Kps3 cells, whereas there was little decrease in the UVSSA-corrected Kps3 cells (**Fig. 4c**). These results indicate

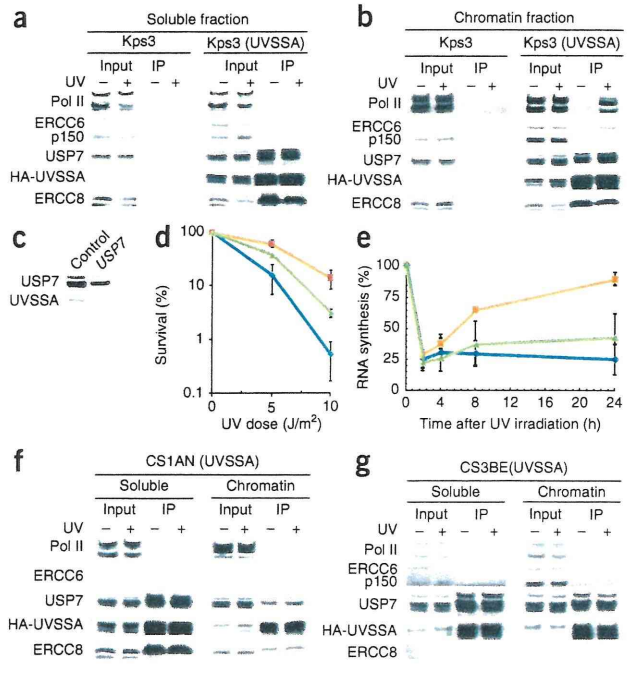

Figure 3 Interaction of UVSSA with RNA Pol II, ERCC6, ERCC8 and USP7. (**a**,**b**) Parental Kps3 cells and Flag- and HA-tagged wild-type UVSSA-corrected Kps3 cells were either irradiated with 20 J/m^2 of UV or were not irradiated and were incubated for 30 min. The UVSSA protein complex (IP) was then affinity purified from the soluble (**a**) or chromatin (**b**) fraction of each cell extract using anti-FLAG M2 agarose and anti-HA agarose and was subjected to protein blotting with antibodies to HA (UVSSA), RNA Pol II, ERCC6, ERCC8 and USP7. p150 corresponds to the CPFP protein (fusion protein consisting of N-terminal ERCC6$^{1-465}$ and the piggyback transposon)[32]. (**c**) Protein blot analysis of USP7 and UVSSA in UVSSA-corrected Kps3 cells and in isogenic cells transfected with *USP7* siRNA. The upper band of USP7 may be a modified form. (**d**) UV survival of parental Kps3 cells (blue rhombuses), UVSSA-corrected Kps3 cells (orange squares) and UVSSA-corrected Kps3 cells transfected with *USP7* siRNA (green triangles). Error bars, s.d. calculated from three independent experiments. (**e**) RNA synthesis after 10 J/m^2 of UV irradiation in the three cell lines in **d**. The symbols for each cell line are the same as in **d**. (**f**) Interaction of UVSSA with RNA Pol II, ERCC8 and USP7 in CS-B cells. Flag- and HA-tagged UVSSA protein was expressed in CS1AN (CS-B) cells, and immunoprecipitation of the cell extracts was performed using antibodies to Flag and HA. (**g**) Interaction of UVSSA with RNA Pol II, ERCC6 and USP7 in CS-A cells. Flag- and HA-tagged UVSSA protein was expressed in CS3BE (CS-A) cells, and immunoprecipitation of the cell extracts was performed using antibodies to Flag and HA. Error bars, s.d. calculated from three independent experiments.

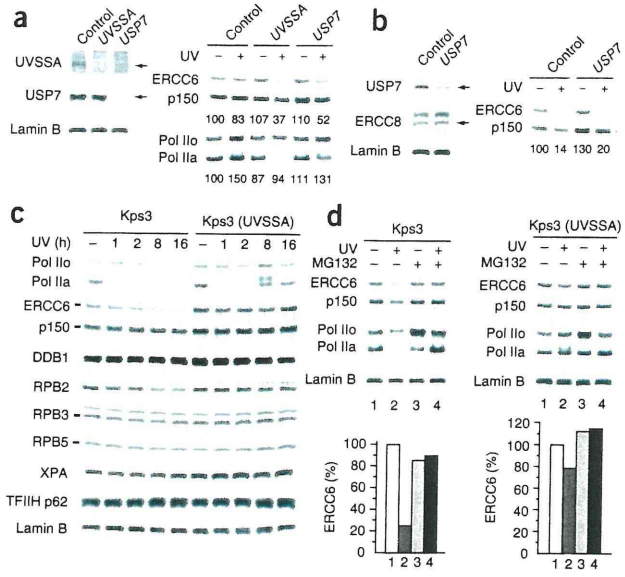

Figure 4 Degradation of ERCC6 in parental Kps3 cells, UVSSA-corrected Kps3 cells and normal cells transfected with *USP7* siRNA after UV irradiation. (**a**) UV-induced degradation of ERCC6 and RNA Pol IIo in normal cells transfected with control siRNA or siRNA targeting *UVSSA* or *USP7*. Knockdown of *UVSSA* and *USP7* was confirmed by protein blotting of cell lysates using the indicated antibodies. Normal cells transfected with each siRNA were irradiated with 10 J/m^2 of UV or not irradiated and were incubated for 16 h. Samples lysed with SDS gel-loading buffer were then analyzed by protein blotting with antibody to ERCC6. Numbers below the blots indicate the amounts of ERCC6 (upper) and RNA Pol IIo (lower) relative to their amounts in non-irradiated normal cells transfected with control siRNA. (**b**) UV-induced degradation of ERCC6 in Kps3 cells transfected with control siRNA or with siRNA targeting *UVSSA* or *USP7*. Knockdown by siRNA and protein blotting were performed as in **c**, except for an 8-h incubation after UV irradiation. Numbers below the blot indicate the amount of ERCC6 relative to the amount in non-irradiated Kps3 cells transfected with control siRNA. (**c**) Parental Kps3 cells and UVSSA-corrected Kps3 cells were irradiated with 10 J/m^2 of UV and incubated for the indicated times. Samples lysed with SDS gel-loading buffer were analyzed by protein blotting using the indicated antibodies. DDB1, UV-damaged DNA binding protein 1; RPB2, second largest subunit of RNA Pol II; RPB3, third largest subunit of RNA Pol II; RPB5, fifth largest subunit of RNA Pol II; XPA, xeroderma pigmentosum group A protein. Only RPB2 was decreased to some extent in UV-irradiated Kps3 cells. (**d**) Inhibition of the degradation of ERCC6 and the reappearance of RNA Pol IIa after UV irradiation in Kps3 cells in the presence of MG132. Parental Kps3 cells and UVSSA-corrected Kps3 cells were either irradiated with 10 J/m^2 of UV or not irradiated and were incubated for 8 h in the presence (10 μM) or absence of the proteasome inhibitor MG132. Samples lysed with SDS gel-loading buffer were analyzed by protein blotting using the indicated antibodies. Histograms indicate the amount of ERCC6 relative to the amount in non-irradiated cells in the absence of MG132.

that UVSSA has an important role in stabilizing ERCC6 in TCR. In addition, ERCC6 was degraded in the *USP7* siRNA–treated cells, as in the *UVSSA* siRNA–treated cells, but not in control siRNA–treated cells (**Fig. 4a**). Kps3 cells that lack *UVSSA* were then treated with *USP7* siRNA. No significant difference in UV-induced degradation of ERCC6 was detected between control siRNA– and *USP7* siRNA–treated Kps3 cells (**Fig. 4b**). These results indicate that UVSSA and USP7 cooperate to protect ERCC6 from UV-induced degradation in TCR.

When the Kps3 cells were UV irradiated in the presence of the proteasome inhibitor MG132, the reduction in ERCC6 levels after UV irradiation was suppressed, and RNA Pol IIa reappeared 16 h after UV irradiation (**Fig. 4d**). These results suggest that, in UV-irradiated Kps3 cells, ERCC6 is ubiquitinated and degraded by the ubiquitin-proteasome pathway, and the recovery of RNA Pol IIa is blocked, leading to the inhibition of UV-RRS.

The amount of RNA Pol IIo decreased in parental Kps3 cells (**Fig. 4c**) and in *UVSSA* siRNA–treated normal cells (**Fig. 4a**), although the decrease in RNA Pol IIo was not significant compared with that of ERCC6. RNA Pol IIo levels did not decrease in the UVSSA-corrected Kps3 cells and in control siRNA–treated cells (**Fig. 4a,c**). In the *USP7* siRNA–treated cells, the amount of RNA Pol IIo slightly decreased after UV irradiation when compared to the amount in control siRNA–treated cells (**Fig. 4a**). Taken together, these results suggest that UVSSA and USP7 are involved in the stabilization of RNA Pol IIo, but the effect might be indirect.

The affected individuals with the UV^{S}S, UV^{S}1KO and UV^{S}1VI, had homozygous mutations in the *ERCC6* and *ERCC8* genes, respectively[5,6]. This prompted us to examine whether some individuals with Cockayne syndrome features and TCR deficiency have mutations in the *UVSSA* gene. We sequenced the ORF of *UVSSA* in three TCR-deficient Cockayne syndrome cell lines (CS7099, CS6864 and CS2760) that have no mutations in the *ERCC6* and *ERCC8* genes. We found only SNPs in *UVSSA* in these cells (**Supplementary Fig. 7**), suggesting that there are some other gene(s) involved in the Cockayne syndrome phenotype beyond *ERCC6* and *ERCC8*. To exclude the possibility that some individuals with Cockayne syndrome have mutations in *UVSSA*, it is necessary to sequence the *UVSSA* ORF in many other TCR-deficient subjects with Cockayne syndrome.

It has been reported that CS-A and CS-B cells are hypersensitive to treatment with hydrogen peroxide and potassium bromate, specific inducers of oxidative DNA damage, and are deficient in the repair of oxidative DNA damage, whereas Kps3 (UV^{S}SA) and UV^{S}S1VI (UV^{S}S/CS-A) cells are not hypersensitive to oxidative DNA damage[6,21,22]. It has also been reported that transcription by RNA Pol II was reduced in the extracts of CS-A and CS-B cells compared to transcription levels in normal cells[23,24]. Nuclear extracts of CS-B cells failed to transcribe human rDNA, whereas those of CS-B cells expressing wild-type ERCC6 showed high transcriptional activity of RNA Pol I (ref. 25). Of note, RNA Pol I transcription was proficient in UV^{S}1KO (UV^{S}S/CS-B) cells[26]. Taken together, these results suggest that marked differences in the pathological phenotypes between Cockayne syndrome and UV^{S}S are caused by differences in transcription and/or in the repair of oxidative DNA damage in affected individuals.

We also determined that ERCC6 was ubiquitinated and degraded by the ubiquitin-proteasome pathway after UV irradiation in Kps3 cells (**Fig. 4c,d**). It has been reported that ERCC6 is required for the resumption of transcription after UV irradiation and for the recruitment of RNA Pol II and other transcription factors at the promoter in UV-irradiated cells[27]. It is therefore suggested that the ubiquitination and degradation of ERCC6 in the absence of UVSSA prevents recovery of RNA Pol IIa after UV irradiation and, consequently, blocks UV-RRS (**Supplementary Fig. 8**). Kps3 cells are deficient in the removal of UV damage on transcribed DNA strands[28], indicating that UVSSA is also required for excision of DNA damage in TCR (**Supplementary Fig. 8**).

It is not yet clear which E3 ligase is involved in the ubiquitination of ERCC6 in TCR. It would be interesting to examine whether ERCC6 is ubiquitinated by ERCC8 (ref. 29), BRCA1-BARD1 (ref. 30) or the p44 subunit of TFIIH[31]. UVSSA may negatively regulate E3 ligase activities. Alternatively or simultaneously, it may positively regulate

the deubiquitinase activity of USP7 to stabilize ERCC6 in TCR. We conclude that the UVSSA-USP7 complex has an important role in TCR, whereby it controls the steady-state levels of ERCC6.

METHODS

Methods and any associated references are available in the online version of the paper at http://www.nature.com/naturegenetics/.

Note: Supplementary information is available on the Nature Genetics website.

ACKNOWLEDGMENTS

We thank Y. Iwamoto and I. Kuraoka for their help in DNA sequencing and microcell-mediated chromosome transfer and M. Hoshi for her help in establishing Flp-In cells and performing immunoprecipitation. We also thank M. Yamaizumi (Kumamoto University Medical School) and N.G. Jaspers (Erasmus Medical Centre) for providing Kps3 cells and TA-24 cells, respectively. We thank G. Spivak for critical reading of the manuscript. This work was supported by a Grant-in-Aid for Scientific Research on Innovative Areas from the Ministry of Education, Culture, Sports, Science and Technology (MEXT) of Japan and by Health and Labor Sciences Research Grants for Research on Intractable Diseases (to K.T.). Part of this work was carried out under the Cooperative Research Project Program of the Institute of Development, Aging and Cancer (IDAC) at Tohoku University.

AUTHOR CONTRIBUTIONS

X.Z., K.H., M.S. and K.T. conceived the experiments. K.T. and H.T. established the cell lines. X.Z., K.H. and C.I. performed microcell-mediated chromosome transfer. A.U., K.H. and M.H. performed CGH array analysis. X.Z., M.S. and S.K. performed biochemical analysis. E.G.N. diagnosed Cockayne syndrome patients. K.T., X.Z., K.H., M.S., M.H., T.N. and A.Y. analyzed the data. K.T., X.Z., M.S. and K.H. wrote the manuscript.

COMPETING FINANCIAL INTERESTS

The authors declare no competing financial interests.

Published online at http://www.nature.com/naturegenetics/.
Reprints and permissions information is available online at http://www.nature.com/reprints/index.html.

1. Hanawalt, P.C. & Spivak, G. Transcription-coupled DNA repair: two decades of progress and surprises. *Nat. Rev. Mol. Cell Biol.* **9**, 958–970 (2008).
2. Fousteri, M. & Mullenders, L.H. Transcription-coupled nucleotide excision repair in mammalian cells: molecular mechanisms and biological effects. *Cell Res.* **18**, 73–84 (2008).
3. Spivak, G. UV-sensitive syndrome. *Mutat. Res.* **577**, 162–169 (2005).
4. Itoh, T., Ono, T. & Yamaizumi, M. A new UV-sensitive syndrome not belonging to any complementation groups of xeroderma pigmentosum or Cockayne syndrome: siblings showing biochemical characteristics of Cockayne syndrome without typical clinical manifestations. *Mutat. Res.* **314**, 233–248 (1994).
5. Horibata, K. *et al.* Complete absence of Cockayne syndrome group B gene product gives rise to UV-sensitive syndrome but not Cockayne syndrome. *Proc. Natl. Acad. Sci. USA* **101**, 15410–15415 (2004).
6. Nardo, T. *et al.* A UV-sensitive syndrome patient with a specific *CSA* mutation reveals separable roles for CSA in response to UV and oxidative DNA damage. *Proc. Natl. Acad. Sci. USA* **106**, 6209–6214 (2009).
7. Nagase, T., Kikuno, R., Ishikawa, K., Hirosawa, M. & Ohara, O. Prediction of the coding sequences of unidentified human genes. XVII. The complete sequences of 100 new cDNA clones from brain which code for large proteins *in vitro*. *DNA Res.* **7**, 143–150 (2000).
8. Nicholson, B. & Suresh Kumar, K.G. The multifaceted roles of USP7: new therapeutic opportunities. *Cell Biochem. Biophys.* **60**, 61–68 (2011).
9. Sanford, J.A. & Stubblefield, E. General protocol for microcell-mediated chromosome transfer. *Somat. Cell Mol. Genet.* **13**, 279–284 (1987).
10. Abe, K. *et al.* Contribution of Asian mouse subspecies *Mus musculus molossinus* to genomic constitution of strain C57BL/6J, as defined by BAC-end sequence-SNP analysis. *Genome Res.* **14**, 2439–2447 (2004).
11. Itoh, T., Linn, S., Ono, T. & Yamaizumi, M. Reinvestigation of the classification of five cell strains of xeroderma pigmentosum group E with reclassification of three of them. *J. Invest. Dermatol.* **114**, 1022–1029 (2000).
12. Strausberg, R.L. *et al.* Generation and initial analysis of more than 15,000 full-length human and mouse cDNA sequences. *Proc. Natl. Acad. Sci. USA* **99**, 16899–16903 (2002).
13. Meinhart, A. & Cramer, P. Recognition of RNA polymerase II carboxy-terminal domain by 3′-RNA-processing factors. *Nature* **430**, 223–226 (2004).
14. Steinmetz, E.J., Conrad, N.K., Brow, D.A. & Corden, J.L. RNA-binding protein Nrd1 directs poly(A)-independent 3′-end formation of RNA polymerase II transcripts. *Nature* **413**, 327–331 (2001).
15. Khoronenkova, S.V., Dianova, I.I., Parsons, J.L. & Dianov, G.L. USP7/HAUSP stimulates repair of oxidative DNA lesions. *Nucleic Acids Res.* **39**, 2604–2609 (2011).
16. Schwertman, P. *et al.* UV-sensitive syndrome protein UVSSA recruits USP7 to regulate transcription-coupled repair. *Nat. Genet.* published online (1 April 2012); doi:10.1038/ng.2230.
17. Kamiuchi, S. *et al.* Translocation of Cockayne syndrome group A protein to the nuclear matrix: possible relevance to transcription-coupled DNA repair. *Proc. Natl. Acad. Sci. USA* **99**, 201–206 (2002).
18. Fousteri, M., Vermeulen, W., vanZeeland, A.A. & Mullenders, L.H. Cockayne syndrome A and B proteins differentially regulate recruitment of chromatin remodeling and repair factors to stalled RNA polymerase II *in vivo*. *Mol. Cell* **23**, 471–482 (2006).
19. Saijo, M. *et al.* Functional TFIIH is required for UV-induced translocation of CSA to the nuclear matrix. *Mol. Cell. Biol.* **27**, 2538–2547 (2007).
20. Rockx, D.A. *et al.* UV-induced inhibition of transcription involves repression of transcription initiation and phosphorylation of RNA polymerase II. *Proc. Natl. Acad. Sci. USA* **97**, 10503–10508 (2000).
21. Spivak, G. & Hanawalt, P.C. Host cell reactivation of plasmids containing oxidative DNA lesions is defective in Cockayne syndrome but normal in UV-sensitive syndrome fibroblasts. *DNA Repair (Amst.)* **5**, 13–22 (2006).
22. D'Errico, M. *et al.* The role of CSA in the response to oxidative DNA damage in human cells. *Oncogene* **26**, 4336–4343 (2007).
23. Selby, C.P. & Sancar, A. Cockayne syndrome group B protein enhances elongation by RNA polymerase II. *Proc. Natl. Acad. Sci. USA* **94**, 11205–11209 (1997).
24. Dianov, G.L., Houle, J.F., Iyer, N., Bohr, V.A. & Friedberg, E.C. Reduced RNA polymerase II transcription in extracts of cockayne syndrome and xeroderma pigmentosum/Cockayne syndrome cells. *Nucleic Acids Res.* **25**, 3636–3642 (1997).
25. Bradsher, J. *et al.* CSB is a component of RNA pol I transcription. *Mol. Cell* **10**, 819–829 (2002).
26. Lebedev, A., Scharffetter-Kochanek, K. & Iben, S. Truncated Cockayne syndrome B protein represses elongation by RNA polymerase I. *J. Mol. Biol.* **382**, 266–274 (2008).
27. Proietti-De-Santis, L., Drane, P. & Egly, J.M. Cockayne syndrome B protein regulates the transcriptional program after UV irradiation. *EMBO J.* **25**, 1915–1923 (2006).
28. Spivak, G. *et al.* Ultraviolet-sensitive syndrome cells are defective in transcription-coupled repair of cyclobutane pyrimidine dimers. *DNA Repair (Amst.)* **1**, 629–643 (2002).
29. Groisman, R. *et al.* CSA-dependent degradation of CSB by the ubiquitin-proteasome pathway establishes a link between complementation factors of the Cockayne syndrome. *Genes Dev.* **20**, 1429–1434 (2006).
30. Wei, L. *et al.* BRCA1 contributes to transcription-coupled repair of DNA damage through polyubiquitylation and degradation of Cockayne syndrome B protein. *Cancer Sci.* **102**, 1840–1847 (2011).
31. Takagi, Y. *et al.* Ubiquitin ligase activity of TFIIH and the transcriptional response to DNA damage. *Mol. Cell* **18**, 237–243 (2005).
32. Horibata, K. *et al.* Mutant Cockayne syndrome group B protein inhibits repair of DNA topoisomerase I–DNA covalent complex. *Genes Cells* **16**, 101–114 (2011).

ONLINE METHODS

Cell lines. Kps3, XP24KO and TA-24 cells belong to UV^{S}S-A and were immortalized by simian virus 40 large T antigen and hTERT. FS3 and WI38VA13 are normal human cells. Mouse A9 cells were used as donors in microcell-mediated chromosome transfer. All cell lines used were cultured in DMEM containing 10% FCS, penicillin and streptomycin at 37 °C under 5% CO_2.

UV survival. Cells were inoculated in 10-cm dishes at a density of 1,000–2,000 cells per dish. After 6 h, cells were washed with PBS and irradiated with UV at 0, 5 and 10 J/m^2. Cells were then incubated for 1–2 weeks. Resulting colonies were fixed with 3.7% formaldehyde and stained with 0.1% crystal violet and were counted using a binocular microscope.

Microcell-mediated chromosome transfer. Donor A9 cells were plated onto 25-cm^2 flasks in DMEM supplemented with 10% FCS. After 1–3 d (when cells were 80% confluent), the culture medium was changed to DMEM supplemented with 20% FCS and 50 ng/ml colcemid (Sigma). After 48 h of incubation, flasks were centrifuged at 12,000*g* for 1 h in the presence of 10 μg/ml cytochalasin B (Sigma) for enucleation. The microcell pellets were resuspended in serum-free DMEM and sequentially filtered through polycarbonate membranes with pores of 8, 5 and 3 μm in diameter. Purified microcells, which were irradiated with 10 Gy of γ-irradiation in some experiments, were plated onto a monolayer of recipient Kps3 cells in a 6-cm dish with serum-free DMEM containing 50 μg/ml phytohemagglutinin P (Sigma). After 30 min of incubation, the microcells were fused with recipient cells by treating the cells with 50% polyethylene glycol 1000 (Nakarai) for 1 min. After fusion, cells were grown for 24 h in DMEM supplemented with10% FCS. Then, cells were replated onto six 10-cm dishes and incubated for 24 h. Cells were irradiated with 10 J/m^2 of UV light. Surviving cells were collected and replated onto six 10-cm dishes and allowed to grow for 7 d. Cells were then irradiated with 10 J/m^2 of UV light. In total, cells were irradiated six times at 7-d intervals. As a negative control, Kps3 cells fused in the absence of microcells were UV irradiated in the same manner.

Comparative genomic hybridization array analysis. The regions of segmented mouse chromosomes transferred to Kps3 cells were analyzed using a Mouse Genome CGH 244A Oligo Microarray Kit with SurePrint Technology (Agilent Technologies), according to the manufacturer's instructions with some modifications. In brief, genomic DNA derived from the 15A-7, KAGB2-4, KAGA2-6 and KAB1-14 clones was compared with genomic DNA from parental Kps3 cells on the arrays. Genomic DNA was extracted by Qiagen Gentra Puregene core Kit A. After digestion with AluI and RsaI, the genomic DNA derived from Kps3 cells was labeled with Cy3, and the genomic DNA from the 15A-7, KAGB2-4, KAGA2-6 and KAB1-14 clones was labeled with Cy5, using a Genomic DNA Enzymatic Labeling Kit (Agilent Technologies). To prevent nonspecific hybridization of human genomic DNA on the array, 50 μg of human Cot-1 DNA (Invitrogen) and 5 μg of mouse Cot-1 DNA (Invitrogen) were mixed and subjected to prehybridization. After hybridization with the labeled genomic DNA, arrays were washed and scanned with GenePix4000B. Scanned data were analyzed by Feature Extraction Software version 9.5 and DNA Analytics version 4.0 (both from Agilent Technologies).

Transfection of mouse BACs. Mouse BAC clones were amplified in *Escherichia coli* cultured in LB medium containing chloramphenicol (25 μg/ml). BAC DNA was prepared with a Midiprep Kit (Qiagen), following the manufacturer's instructions. BAC DNA (20 μg) was cotransfected with 0.6 μg of pSV2neo into recipient Kps3 cells grown on a 10-cm tissue culture dish, and cells were selected with medium containing G418 (400 μg/ml) and irradiated with 10 J/m^2 of UV twice at 4–d intervals to examine whether the BAC-transfected Kps3 clones acquired a normal level of UV resistance.

Recovery of RNA synthesis after UV irradiation. To measure RNA synthesis after UV irradiation, two sets of cells were seeded into 6-well culture plates (1×10^6 cells/well). One set was used for counting cells and the other for measuring RNA synthesis. After 6 h of incubation, cells were washed with PBS and treated with UV at 10 J/m^2. After 2, 4, 8 and 24 h of incubation, the number of cells in one set was counted. The other set of cells was washed with PBS and incubated in DMEM containing 370 kBq/ml of [^{3}H]-uridine for 30 min to quantify RNA synthesis. Labeling was terminated by the addition of sodium azide to a final concentration of 200 μg/ml. Cells were washed twice with PBS containing 200 μg/ml sodium azide and lysed in 0.8% SDS for 30 min at room temperature. An equal volume of 10% trichloroacetic acid containing 0.1 M sodium pyrophosphate was then added to the lysates, and these were incubated on ice for 1 h. Acid-insoluble materials were collected on GF-C glass microfiber filters (Whatman), and radioactivity was measured with an LS 6500 liquid scintillation counter (Beckman Coulter). Total radioactivity was divided by the number of cells to obtain single-cell radioactivity. The ratio (as a percentage) of the radioactivity of individual UV-irradiated cells to that of non-irradiated cells was considered as a measure of the recovery of RNA synthesis after UV irradiation (UV-RRS).

Immunoprecipitation. Cells stably expressing a Flag- and HA-tagged protein were lysed with MNase buffer (20 mM Tris-HCl, pH 7.5, 100 mM KCl, 300 mM sucrose, 2 mM $MgCl_2$, 0.1% Triton X-100, 1 mM $CaCl_2$, 1 mM DTT and complete protease inhibitor cocktail (Roche)) at 4 °C for 10 min. Lysates were centrifuged at 3,800*g* for 5 min. Supernatant was used as the soluble fraction. The pellet was washed once with MNase buffer and incubated with 30 U/ml of micrococcal nuclease (Takara) in MNase buffer at 25 °C for 30 min. The reaction was terminated by adding EDTA to a 5 mM final concentration and centrifuged at 3,800*g* for 5 min at 4 °C. The pellet was washed with MNase buffer. Supernatants were combined and used as the solubilized chromatin fraction. Tagged protein was affinity purified from the soluble and solubilized chromatin fractions with anti-FLAG M2 antibody-conjugated agarose (Sigma) followed by anti-HA agarose (Sigma).

Knockdown experiments. siRNA (Thermo Scientific) was transfected into target cells with RNAiMAX (Invitrogen), according to the manufacturer's instructions. At 24 h after the first transfection, a second transfection was performed. Cells were allowed to grow for another 36 h before experiments were carried out.

Quantitative RT-PCR. cDNA was synthesized from fresh total RNA using a Quantitative Reverse Transcription kit (Qiagen), following the manufacturer's instructions. RT-PCR samples were prepared with TaqMan gene expression master mix (Applied Biosystems), according to the manufacturer's instructions. RT-PCR was carried out using the 7300 Real-Time PCR system (Applied Biosystems), under the following conditions: 10 s at 95 °C, 10 s at 60 °C and 20 s at 72 °C for 25 cycles. Probe sets were ordered from Applied Biosystems.

UV-induced translocation of ERCC8 to the nuclear matrix using a cell-free system. UV-induced translocation of ERCC8 in the cell-free system was examined as described previously[19]. Parental Kps3 cells and UVSSA-corrected Kps3 cells were irradiated with 20 J/m^2 of UV and incubated for 1 h and then treated with CSK-Triton buffer (10 mM PIPES, pH 6.8, 100 mM NaCl, 300 mM sucrose, 3 mM $MgCl_2$, 0.5% Triton X-100, 1 mM DTT, 1 mM EGTA and Complete protease inhibitor cocktail (Roche)) to prepare the insoluble (CSK-ppt) fractions. The soluble fractions (CSK-sup) were prepared from CS3BE (CS-A) cells stably expressing Flag- and HA-tagged ERCC8 by treatment with CSK-Triton buffer. The CSK-sup fraction containing HA-tagged ERCC8 was incubated with the CSK-ppt fraction and then treated with DNase I. The ERCC8 retained in the DNase I–insoluble fractions was detected by immunoblotting with antibody to HA.

Antibodies. The antibodies employed were to ERCC8 (W-16, Santa Cruz Biotechnology), ERCC6 (E-18, Santa Cruz Biotechnology), RNA Pol II (N-20 and A-10, Santa Cruz Biotechnology), KIAA1530 (106751, GeneTex) and HA (3F10, Roche).

ACS Chemical Neuroscience

Research Article

pubs.acs.org/acschemicalneuroscience

Discovery of a Tamoxifen-Related Compound that Suppresses Glial L-Glutamate Transport Activity without Interaction with Estrogen Receptors

Kaoru Sato,*[,‡,†] Jun-ichi Kuriwaki,[‡,†] Kanako Takahashi,[‡] Yoshihiko Saito,[§] Jun-ichiro Oka,[§] Yuko Otani,[∥] Yu Sha,[∥] Ken Nakazawa,[‡] Yuko Sekino,[‡] and Tomohiko Ohwada*[,∥]

[‡]Laboratory of Neuropharmacology, Division of Pharmacology, National Institute of Health Sciences, 1-18-1 Kamiyoga, Setagaya-ku, Tokyo 158-8501, Japan

[§]Laboratory of Pharmacology, Faculty of Pharmaceutical Sciences, Tokyo University of Science, 2541 Yamazaki, Noda-city, Chiba 278-8510, Japan

[∥]Laboratory of Organic and Medicinal Chemistry, Graduate School of Pharmaceutical Sciences, University of Tokyo, 7-3-1, Hongo, Bunkyo-ku, Tokyo 113-0033, Japan

ABSTRACT: We recently found that tamoxifen suppresses L-glutamate transport activity of cultured astrocytes. Here, in an attempt to separate the L-glutamate transporter-inhibitory activity from the estrogen receptor-mediated genomic effects, we synthesized several compounds structurally related to tamoxifen. Among them, we identified two compounds, **1** (YAK01) and **3** (YAK037), which potently inhibited L-glutamate transporter activity. The inhibitory effect of **1** was found to be mediated through estrogen receptors and the mitogen-activated protein kinase (MAPK)/phosphatidylinositol 3-kinase (PI3K) pathway, though **1** showed greatly reduced transactivation activity compared with that of 17β-estradiol. On the other hand, compound **3** exerted its inhibitory effect through an estrogen receptor-independent and MAPK-independent, but PI3K-dependent pathway, and showed no transactivation activity. Compound **3** may represent a new platform for developing novel L-glutamate transporter inhibitors with higher brain transfer rates and reduced adverse effects.

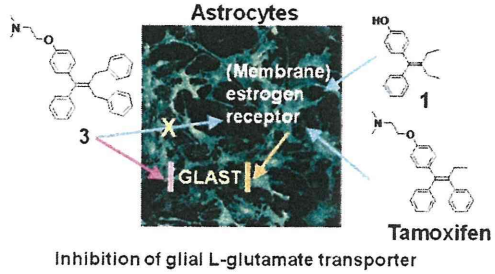

Inhibition of glial L-glutamate transporter

KEYWORDS: *Tamoxifen, astrocyte, L-glutamate transporter, ERα, tetrasubstituted ethylene, nongenomic pathway*

L-Glutamate (L-Glu) is one of the major excitatory neurotransmitters in the central nervous system (CNS), but high concentrations of extracellular L-Glu cause excessive stimulation of L-Glu receptors in the CNS, leading to neurotoxicity.[1,2] Astrocyte L-Glu transporters are the only machinery available to remove L-Glu from extracellular fluid and to maintain a low and nontoxic concentration of L-Glu.[3] Consequently, dysfunction of astrocyte L-Glu transporters is considered to be implicated in the pathology of neurodegenerative conditions.[4] Therefore, exogenous compounds that can regulate the function of L-Glu transporters may provide chemical tools to investigate the regulatory mechanisms of these transporters at the molecular level, and would also be candidate therapeutic agents.

There is growing evidence that estrogen receptor (ER) α, which is a nuclear ER (nER) that mediates genomic effects, can also be translocated to plasma membranes and mediate acute nongenomic effects in some cases. We have clarified that 17β-estradiol (E2) inhibits L-Glu transporters via a nongenomic pathway involving membrane-associated ERα (mERα).[5] Tamoxifen (Tam), a synthetic estrogen analogue that is clinically used in the treatment of breast cancer to block the proliferative action of estrogens,[6] also inhibited astrocyte L-Glu transporters at picomolar concentration, probably through the same nongenomic pathway as E2.[7] Because overexpression of astrocyte L-Glu transporters is often associated with neuropsychiatric disorders,[4] inhibitors of L-Glu transporters may be clinically useful to ameliorate these disorders.[8] However, Tam also acts on genomic pathways involving nuclear estrogen receptors (nERs) α and β, depending on the cell type and promoter context,[9] and so may cause adverse effects including endometrial changes, depression and weight gain.[10,11] Therefore, Tam-inspired compounds that retain the inhibitory effect on L-Glu transporters, but lack the nER-mediated genomic effects, would be useful tools for biological research, as well as candidate therapeutic agents.

Tam is a tetrasubstituted triphenylethylene derivative, in which the four substituents on the olefinic carbon atoms are different. This structural complexity makes the stereospecific synthesis of Tam-related derivatives difficult. We thus focused on Tam-inspired compounds bearing identical substituents on at least one of the olefinic carbon atoms.[12] It is well-known that the *N*,*N*-dimethylaminoethyl substituent on the phenolic oxygen atom and the regiochemistry of the tetrasubstituted

Received: September 29, 2011
Accepted: November 14, 2011
Published: November 14, 2011